Electronic Supplementary Information

Photosensitized samarium(III) and erbium(III) complexes of planar *N,N*-donor heterocyclic bases: crystal structures and evaluation of biological activity

Srikanth Dasari, Zafar Abbas, Priyaranjan Kumar and Ashis K. Patra*

Department of Chemistry

Indian Institute of Technology Kanpur, Kanpur-208016, Uttar Pradesh, India

Figure S30: Bar diagram showing Mechanistic photocleavage of SC pUC19 DNA of complexes **1-4** in presence of various additives.	S31

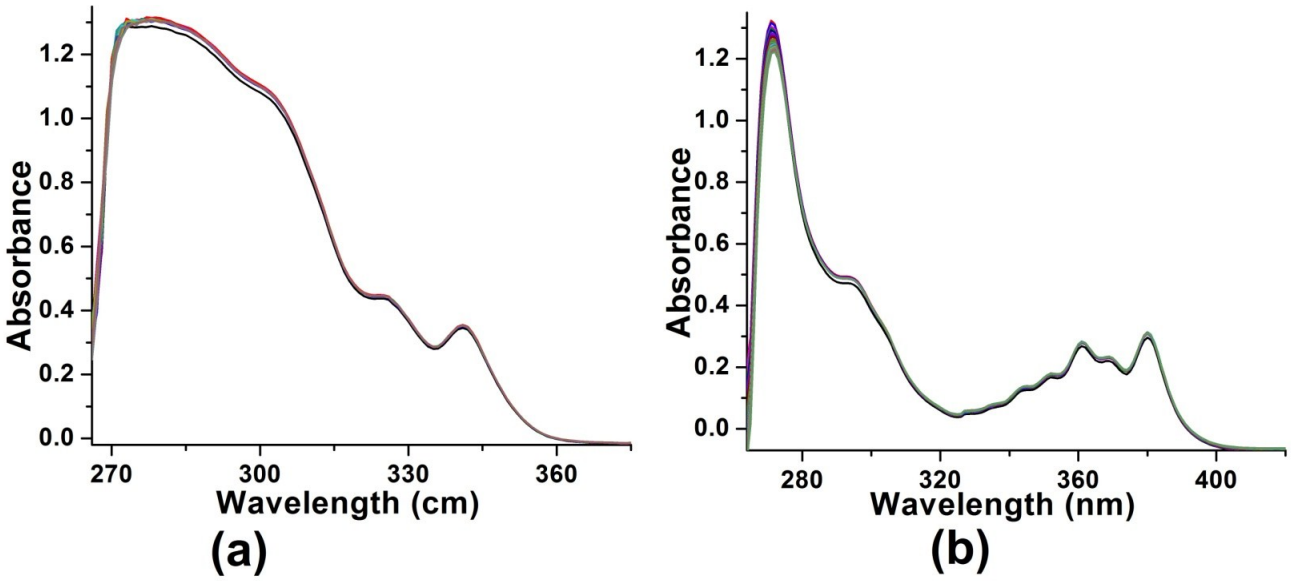

Figure S1: Time-dependent absorption spectral traces of complexes [Sm(dpq)$(DMF)_2(H_2O)Cl_3$](**1**) (100 μM) (a) and [Sm(dppz)$(DMF)_2(H_2O)Cl_3$](**2**) (50 μM) (b) monitored for 4 h in DMF at 25 °C to access the stability of the complexes in solution.

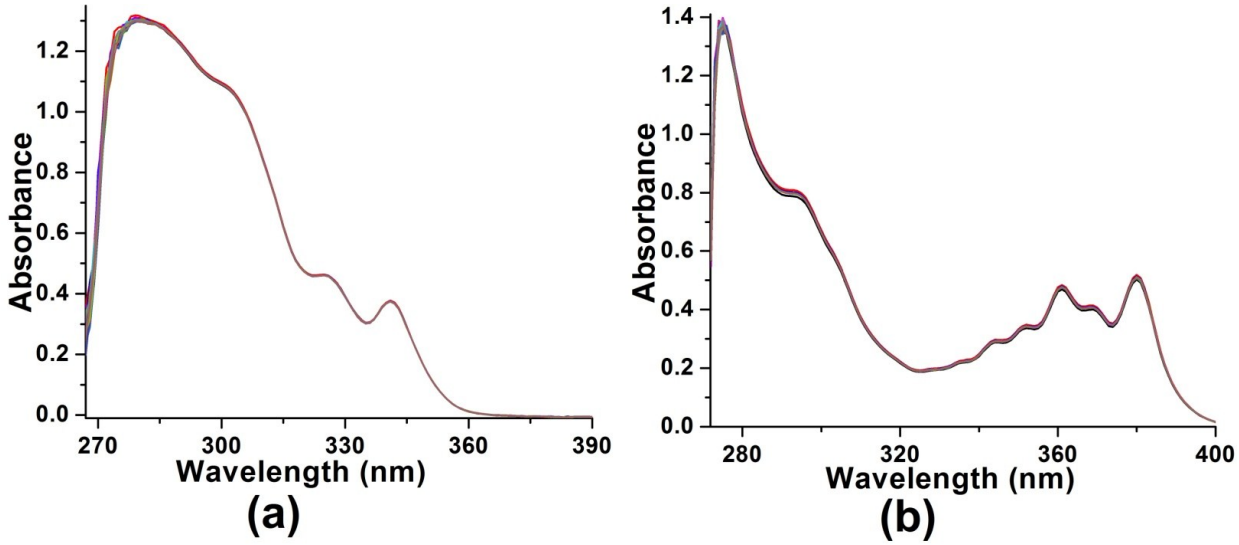

Figure S2: Time-dependent absorption spectral traces of complexes [[Er(dpq)$(DMF)_2Cl_3$] (**3**) (100 μM) (a) and [Er$(dppz)_2Cl_3$] (**4**) (40 μM) (b) monitored for 4 h in DMF at 25 °C to access the stability of the complexes in solution.

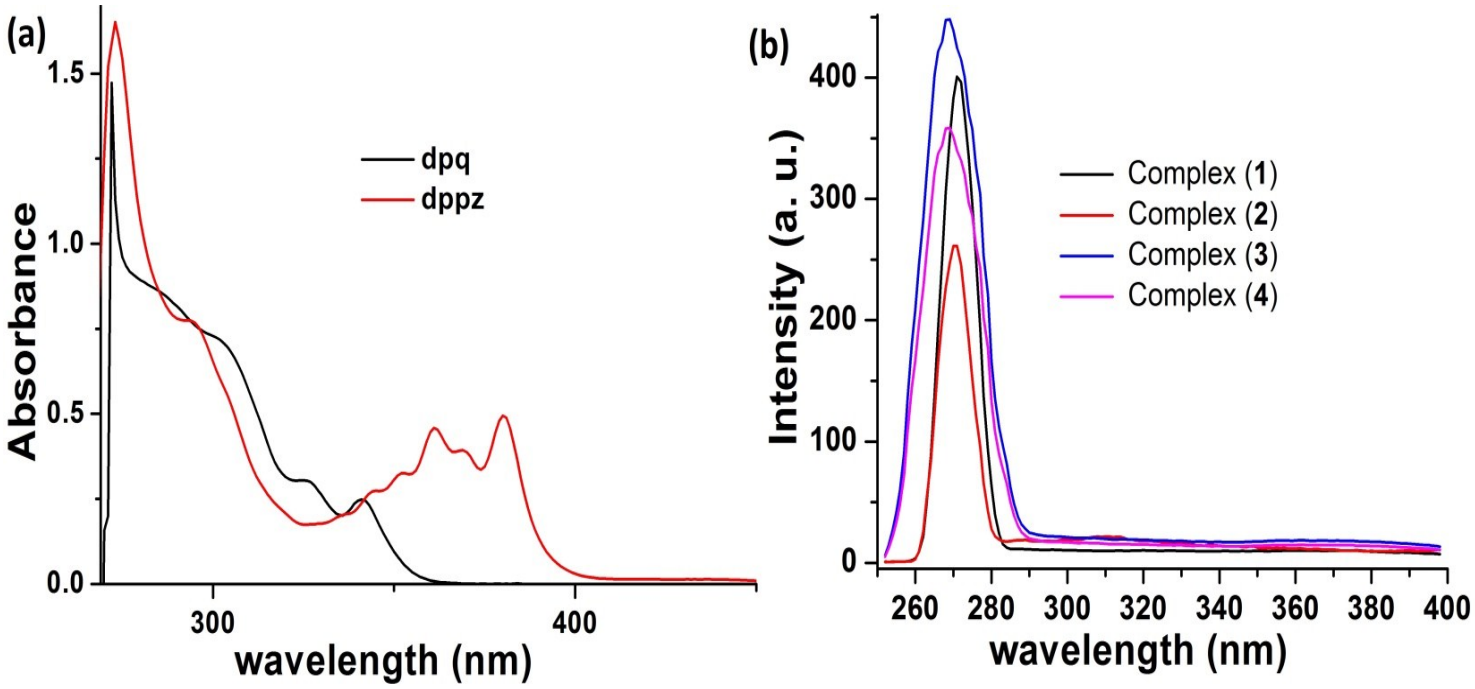

Figure S3. (a) UV-visible spectra of dpq (20 μM) and dppz (15 μM) in DMF. (b) Excitation spectra of the complexes **1**-**4** at 200 μM in DMF in at 298 K. Excitation and emission slit width = 10 nm, λ_{em} = 598 nm for complexes **1** and **2** and λ_{em} = 545 nm for complexes **3** and **4**.

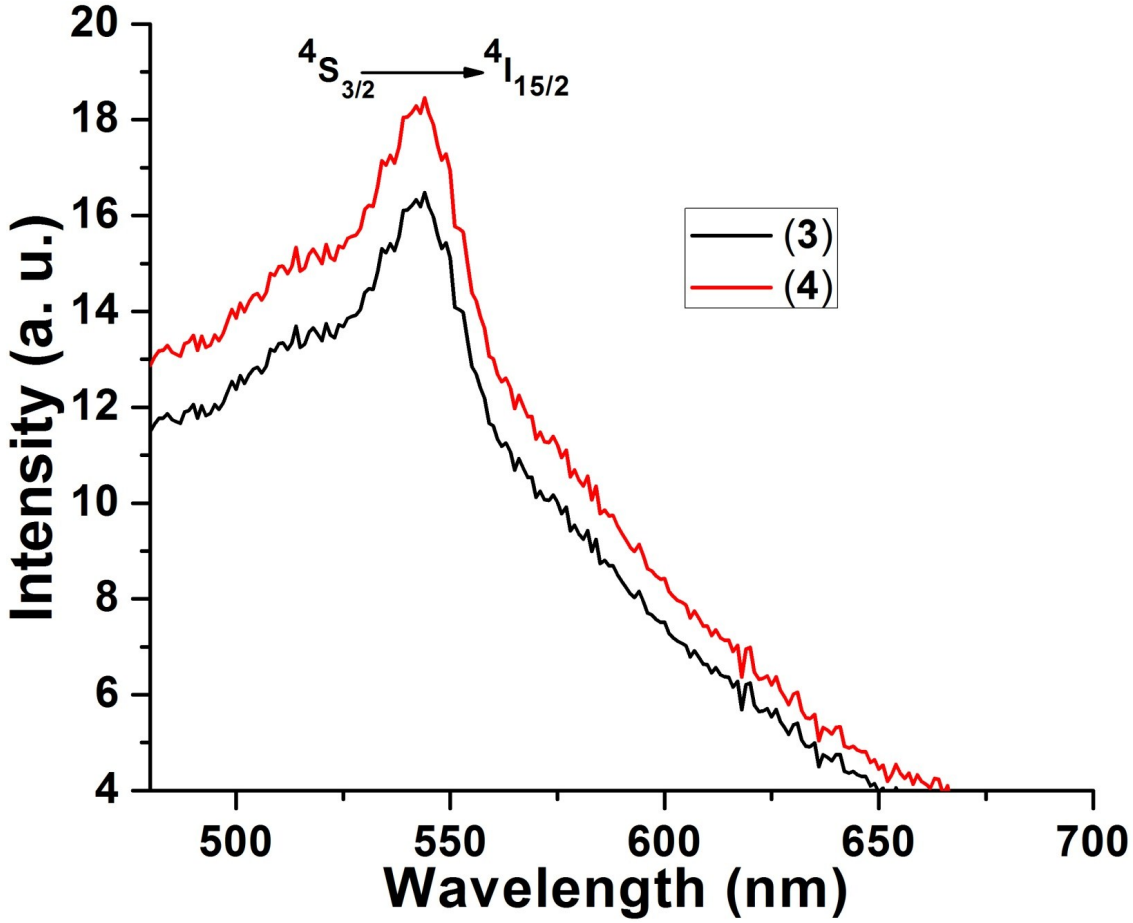

Figure S4. Time-delayed luminescence spectra of [Er(dpq)$(DMF)_2Cl_3$](**3**) (black) and [Er$(dppz)_2Cl_3$](**4**) (red) at 200 μM in DMF (delay time and gate time = 0.1 ms, λ_{ex} = 340 and 380 nm). The corresponding $^4S_{3/2} \rightarrow {}^4I_{15/2}$ transitions are shown on the respective spectra.

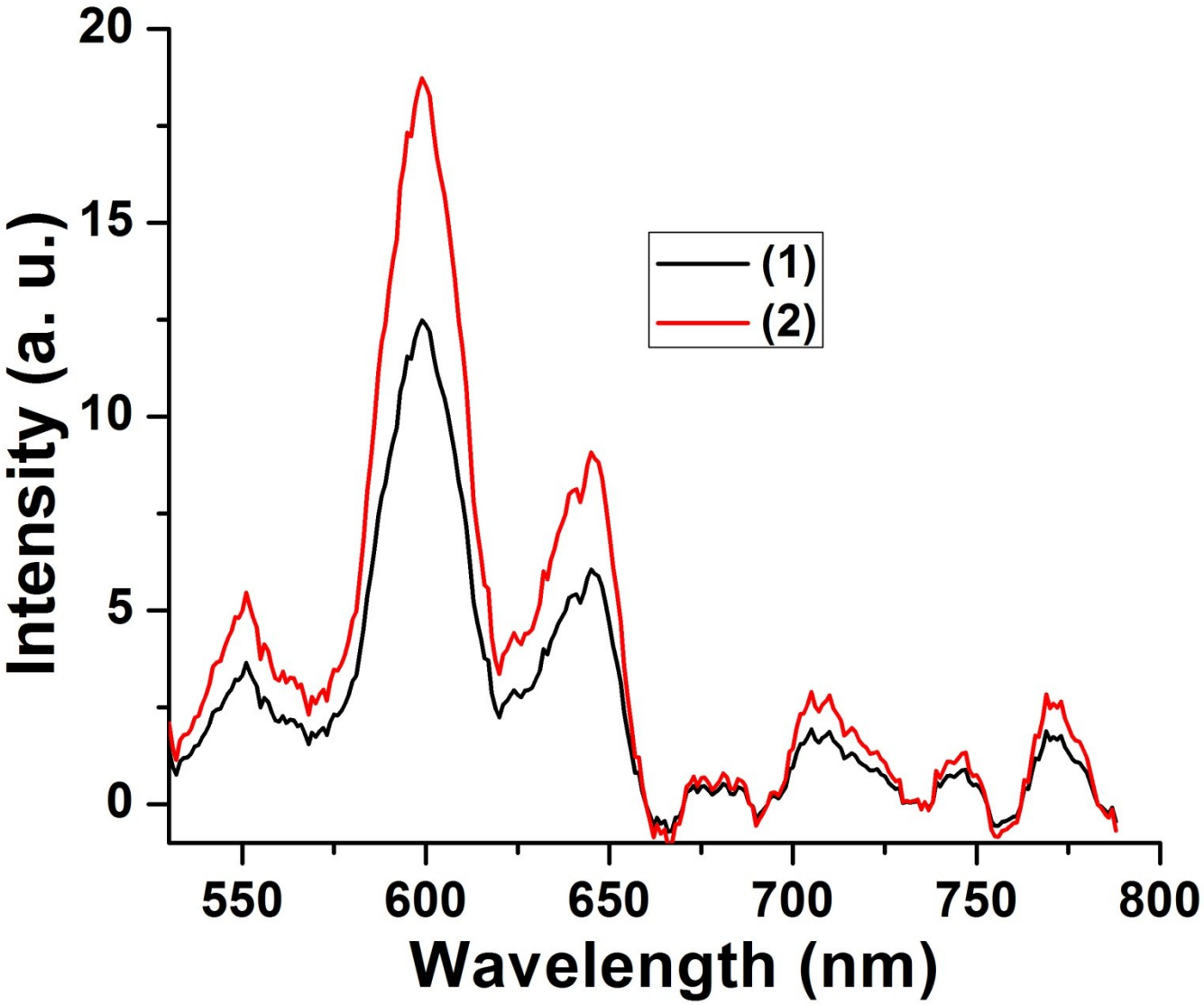

Figure S5. Time-delayed luminescence spectra of $[Sm(dpq)(DMF)_2(H_2O)Cl_3]$ (**1**) (black) and $[Sm(dppz)(DMF)_2(H_2O)Cl_3]$ (**2**) (red) at 200 μM in DMF (delay time and gate time = 0.1 ms, λ_{ex} = 365 nm).

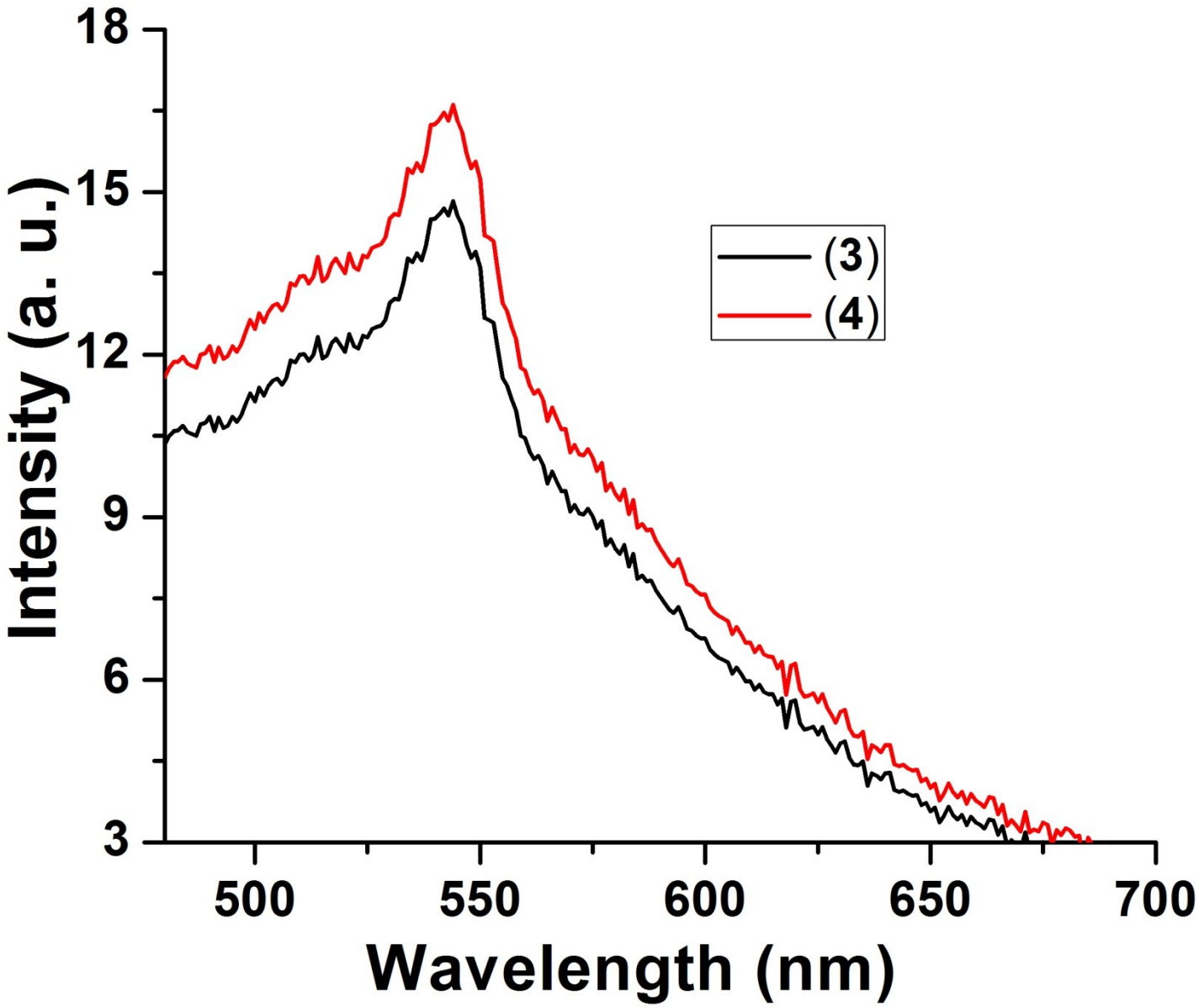

Figure S6. Time-delayed luminescence spectra of [Er(dpq)(DMF)$_2$Cl$_3$](**3**) (black) and [Er(dppz)$_2$Cl$_3$](**4**) (red) at 200 μM in DMF (delay time and gate time = 0.1 ms, λ_{ex} = 365 nm).

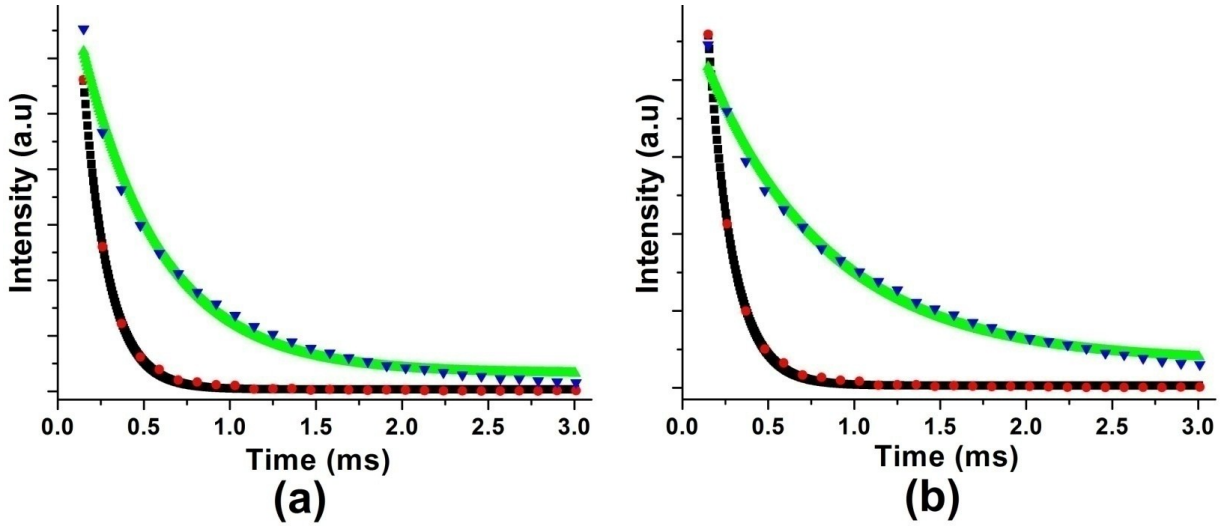

Figure S7. Luminescence decay profile from $^4G_{5/2}$ state and lifetime measurements at 598 nm Sm^{3+} in complexes **1**–**2** (a and b) respectively in H_2O and D_2O under ambient condition at 298 K. λ_{ex}= 340 nm, [complex] = 180 μM, delay time and gate time = 0.1 ms, total decay time = 3.0 ms, Ex. and Em. Slit = 10 nm. The black (in H_2O) and green (in D_2O) curves are the best fits considering single-exponential behavior of the decay.

Luminescence lifetime (τ)[a] and overall quantum yield ($\phi_{overall}$)[b] of the complexes in H_2O and D_2O are shown below.

Complex	λ_{ex}(nm)	τ^{H_2O} (ms)	τ^{D_2O} (ms)	ϕ^{H_2O}	ϕ^{D_2O}	τ^{H_2O}[c] (ms)
1	340	0.14	0.38	0.048	0.320	0.137(aerated) 0.347(degased)
2	380	0.13	0.40	0.0506	0.422	0.126(aerated) 0.369(degased)
3	340	0.10	0.25	0.023	0.204	0.103(aerated) 0.198(degased)
4	380	0.11	0.26	0.017	0.216	0.113(aerated) 0.203(degased)

[a]Luminescence lifetime measured from decay profile from $^4G_{5/2}$ excited state at 598 nm for Sm^{3+} complexes and $^4S_{3/2}$ excited state at 545 nm for Er^{3+} complexes within experimental uncertainty of ±10%. [b]Quinine sulphate was used as a standard for quantum yield calculation, values are within an experimental uncertainty of ±15%. [c] Lifetime measurements of complex **1-4** under aerated and degassed condition.

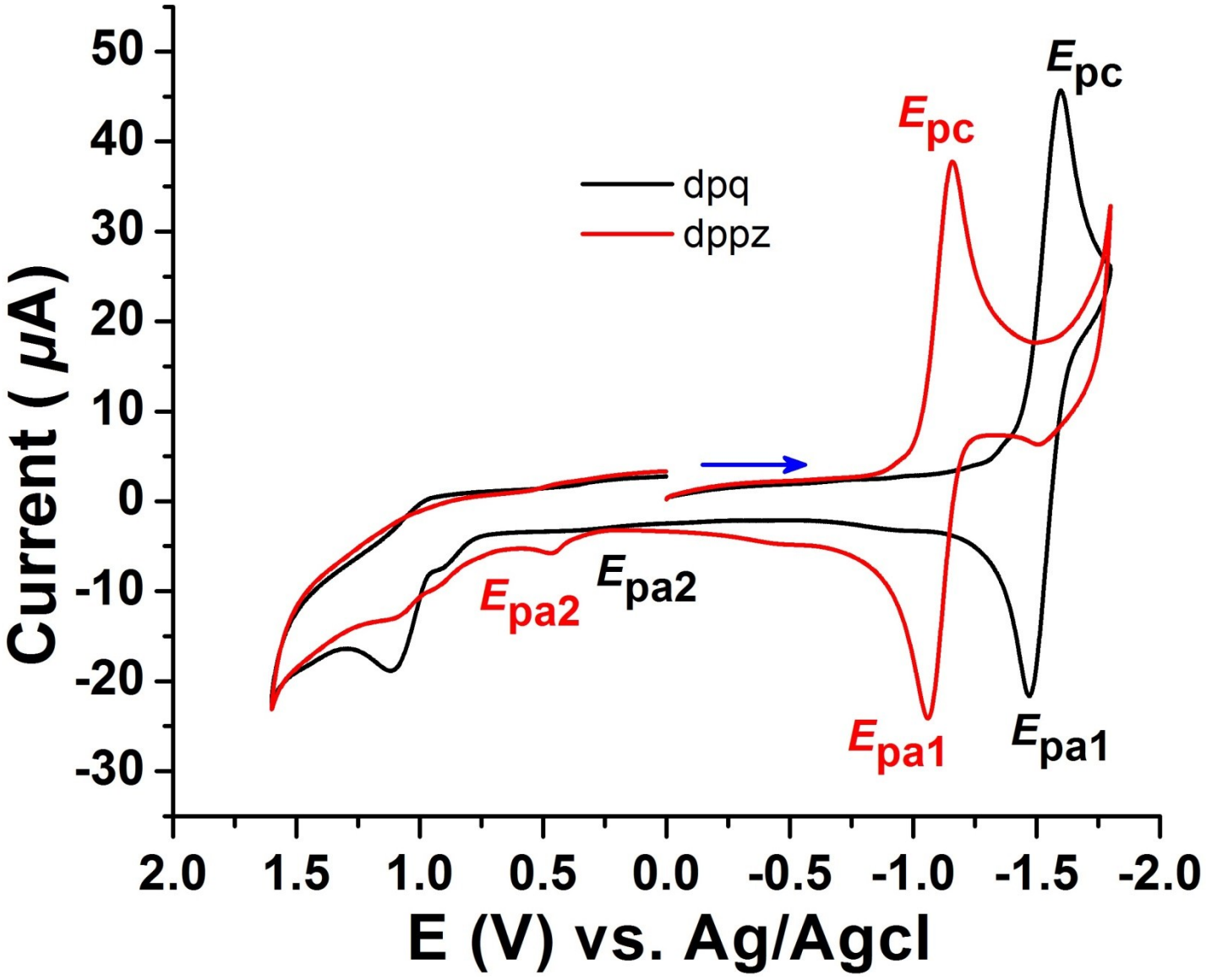

Figure S8. Cyclic voltammograms of the dpq and dppz (1 mM) in DMF-0.1M tertabutylammonium perchlorate (TBAP) as supporting electrolyte at a scan speed of 100 mV s^{-1} at 25 °C.

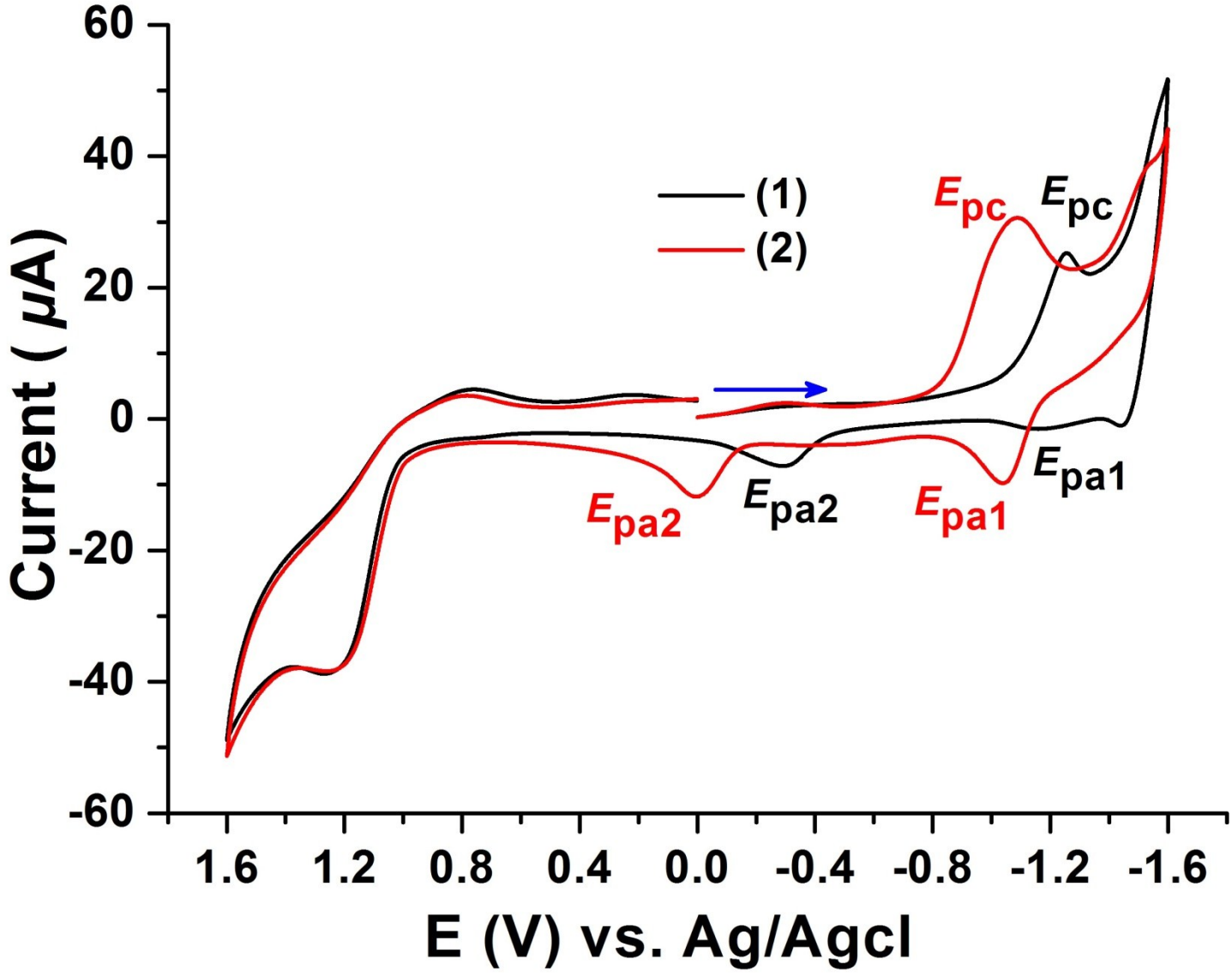

Figure S9. Cyclic voltammograms of the complexes $[Sm(dpq)(DMF)_2(H_2O)Cl_3]$ (**1**) and $[Sm(dppz)(DMF)_2(H_2O)Cl_3]$ (**2**) (1 mM) in DMF-0.1M tertabutylammonium perchlorate (TBAP) as supporting electrolyte at a scan speed of 100 mV s^{-1} at 25 °C.

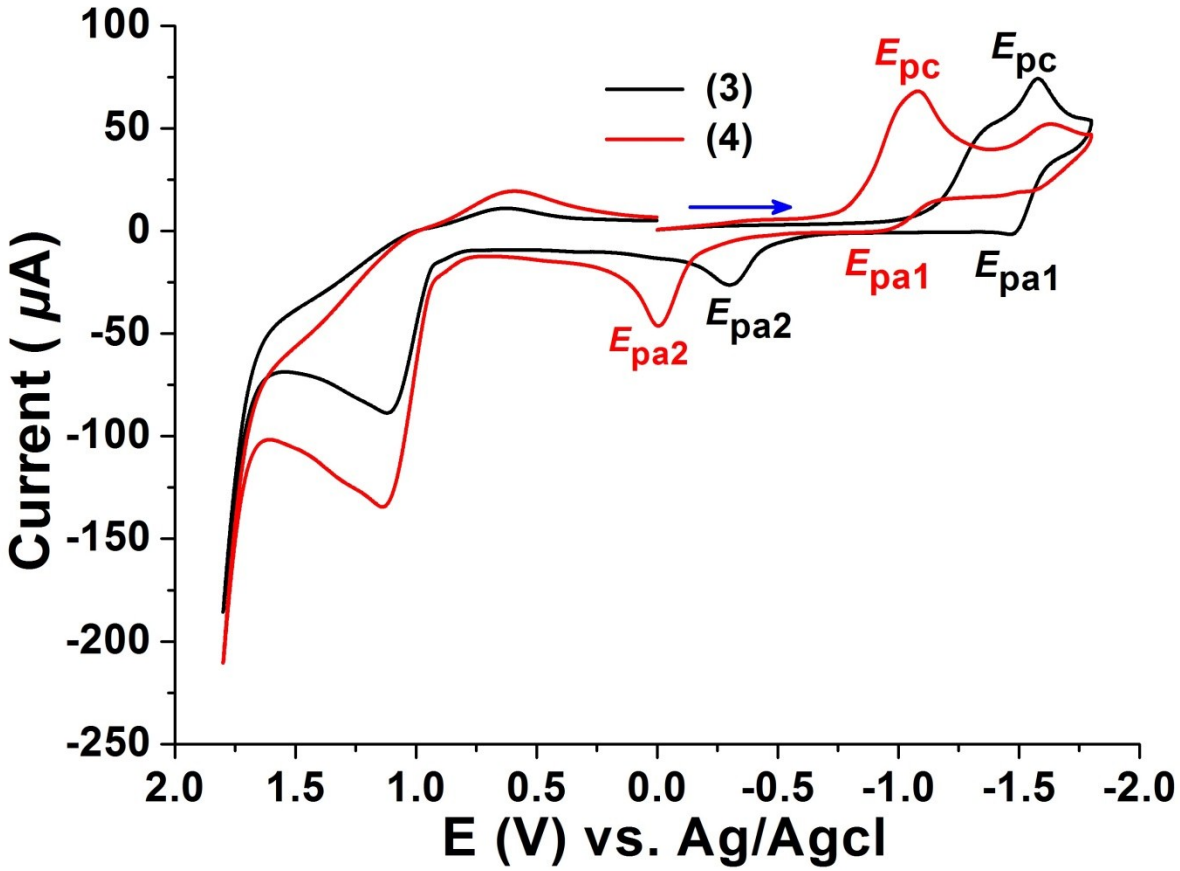

Figure S10. Cyclic voltammograms of the complexes [[Er(dpq)(DMF)$_2$Cl$_3$] (**3**) and [Er(dppz)$_2$Cl$_3$] (**4**) (1 mM) in DMF -0.1M tertabutylammonium perchlorate (TBAP) as supporting electrolyte at a scan speed of 100 mV s^{-1} at 25 °C.

Table. Cyclic voltammetry data of the ligands and complexes **1**-**4**.

Compounds	E_{pc} (V)	E_{pa} (V)	$E_{1/2}$	ΔE_p (V)	i_{pa}/i_{pc}
dpq	-1.582	-1.479	-1.53	-0.103	0.88
		-0.358			
dppz	-1.165	-1.061	-1.113	-0.104	0.90
		-0.464			
1	-1.245	-1.155	-1.20	-0.090	0.40
		-0.324			0.20
2	-1.142	-1.054	-1.098	-0.088	0.71
		-0.016			0.42
3	-1.580	-1.464	-1.522	-0.116	0.50
		-0.304			0.31
4	-1.085	-0.978	-1.0315	-0.107	0.62
		-0.012			0.31

$E_{pc\ and}$ E_{pa} are the cathodic and anodic peak potentials, i_{pa} and i_{pc} are the anodic and cathodic peak currents, $E_{1/2}$ is the half-wave potential respectively.

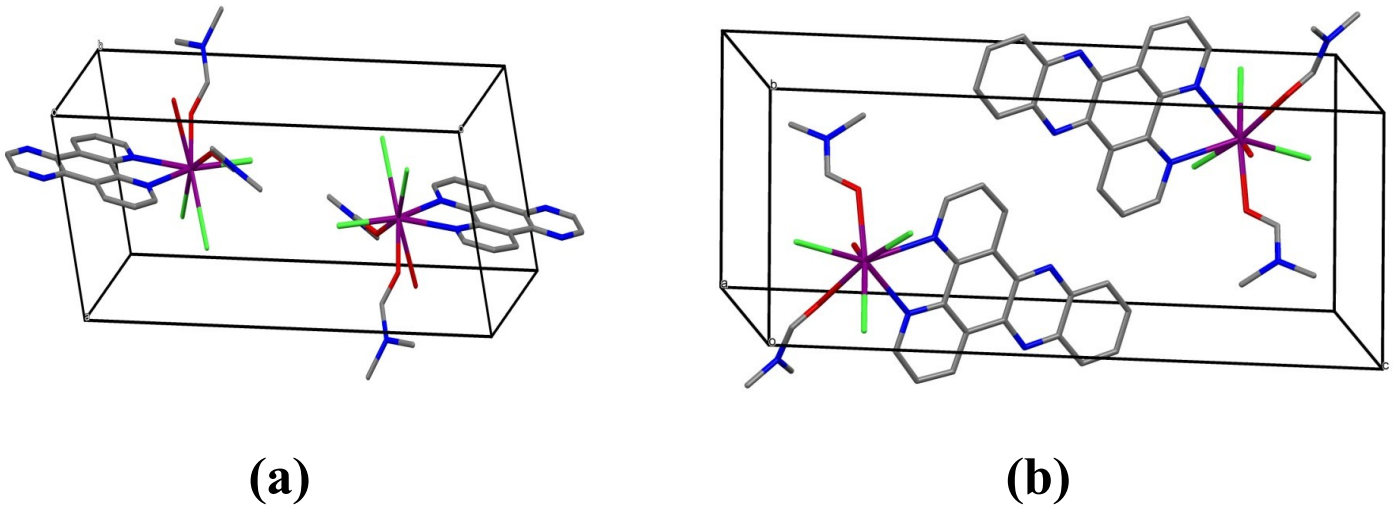

Figure S11. Unit cell packing diagram of complex **1(**a**)** and complex **2**(b).

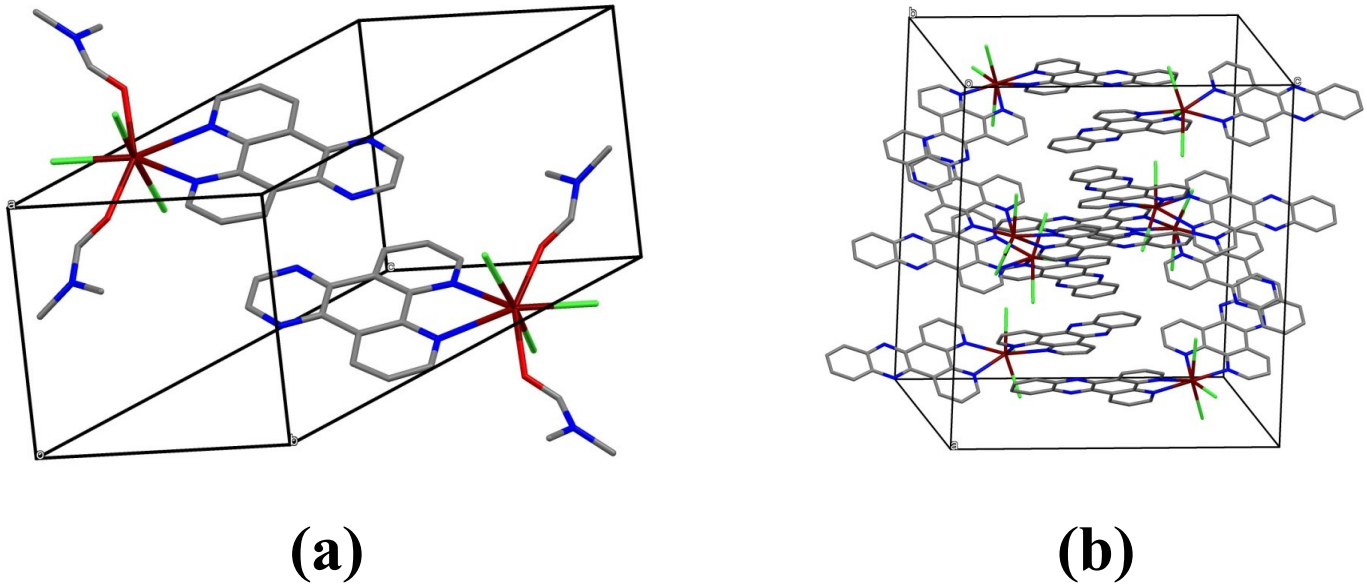

Figure S12. Unit cell packing diagram of complex **3** (a) and complex **4** (b).

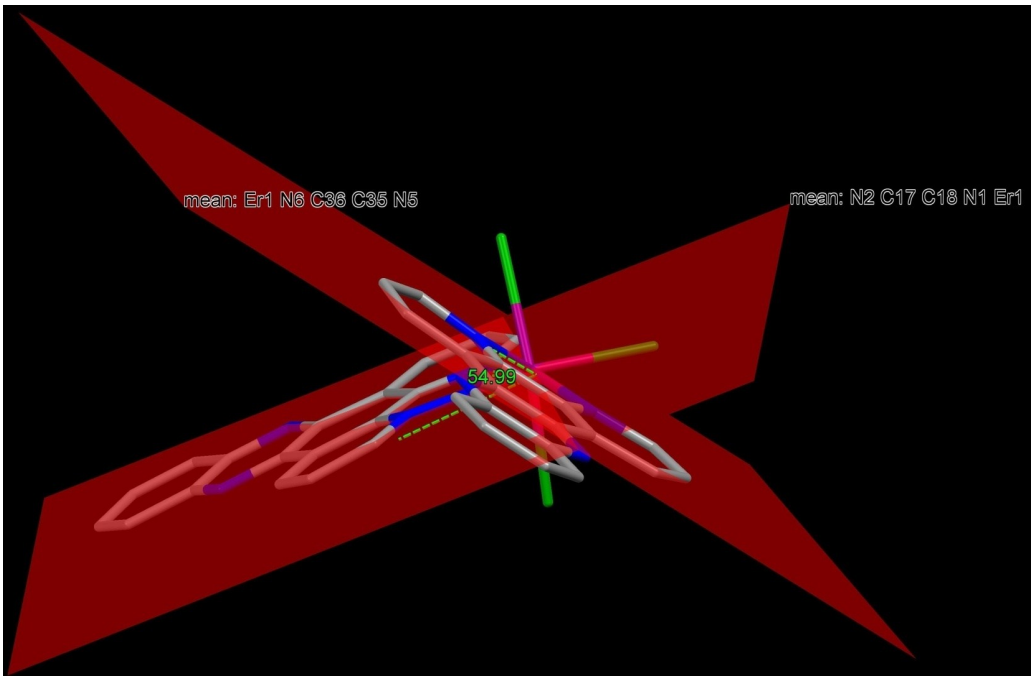

Figure S13. Dihedral angle between the planes of the bound dppz ligands in complex **4**.

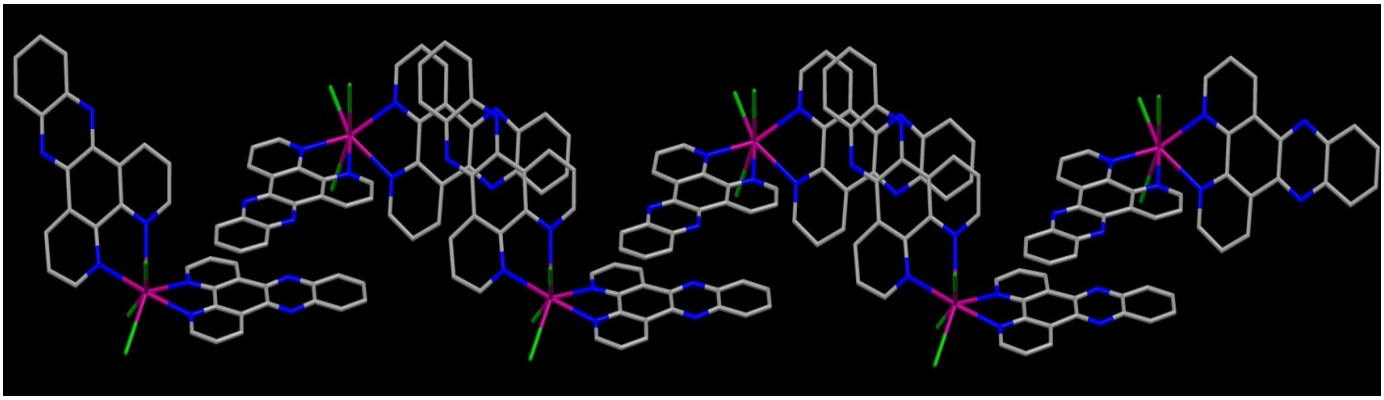

Figure S14. Complex **4** showing favorable π-π stacking interactions to form one dimensional chain.

Table S1: Selected bond lengths (Å) and bond angles (deg) for $[Sm(dpq)(DMF)_2(H_2O)Cl_3]$ (**1**) and $[Sm(dppz)(DMF)_2(H_2O)Cl_3]$ (**2**)

$[Sm(dpq)(DMF)_2(H_2O)Cl_3]$(**1**)		$[Sm(dppz)(DMF)_2(H_2O)Cl_3]$(**2**)	
Bond lengths (Å)		**Bond lengths (Å)**	
Sm(1)-Cl(1)	2.7080(10)	Sm(1)-Cl(1)	2.7134(11)
Sm(1)-Cl(2)	2.8108(8)	Sm(1)-Cl(2)	2.8074(10)
Sm(1)-Cl(3)	2.7767(9)	Sm(1)-Cl(3)	2.7612(10)
Sm(1)- N(1)	2.678(2)	Sm(1)- N(1)	2.687(3)
Sm(1)-N(2)	2.662(2)	Sm(1)-N(2)	2.643(3)
Sm(1)-O(1)	2.419(2)	Sm(1)-O(1)	2.405(3)
Sm(1)-O(2)	2.437(2)	Sm(1)-O(2)	2.424(3)
Sm(1)-O(3)	2.455(2)	Sm(1)-O(3)	2.452(3)
Bond Angles (deg)		**Bond Angles (deg)**	
O(1)-Sm(1)-O(2)	119.15(7)	O(1)-Sm(1)-O(2)	118.95(10)
O(1)-Sm(1)-O(3)	66.55(7)	O(1)-Sm(1)-O(3)	66.91(10)
O(2)-Sm(1)-O(3)	69.33(7)	O(2)-Sm(1)-O(3)	69.36(10)
O(1)-Sm(1)-N(2)	73.30(7)	O(1)-Sm(1)-N(2)	74.66(10)
O(2)-Sm(1)-N(2)	128.64(7)	O(2)-Sm(1)-N(2)	129.68(10)
O(3)-Sm(1)-N(2)	73.11(8)	O(3)-Sm(1)-N(2)	74.68(10)
O(1)-Sm(1)-N(1)	124.65(8)	O(1)-Sm(1)-N(1)	124.68(10)
O(2)-Sm(1)-N(1)	74.42(7)	O(2)-Sm(1)-N(1)	74.56(10)
O(3)-Sm(1)-N(1)	71.38(8)	O(3)-Sm(1)-N(1)	70.77(10)
N(2)-Sm(1)-N(1)	61.03(7)	N(2)-Sm(1)-N(1)	60.85(10)
O(1)-Sm(1)-Cl(1)	79.20(6)	O(1)-Sm(1)-Cl(1)	78.63(7)
O(2)-Sm(1)-Cl(1)	76.78(5)	O(2)-Sm(1)-Cl(1)	75.84(8)
O(3)-Sm(1)-Cl(1)	107.88(6)	O(3)-Sm(1)-Cl(1)	107.08(8)
N(2)-Sm(1)-Cl(1)	149.44(5)	N(2)-Sm(1)-Cl(1)	149.98(7)
N(1)-Sm(1)-Cl(1)	149.29(5)	N(1)-Sm(1)-Cl(1)	148.91(8)
O(1)-Sm(1)-Cl(3)	155.42(5)	O(1)-Sm(1)-Cl(3)	154.81(7)
O(2)-Sm(1)-Cl(3)	78.51(6)	O(2)-Sm(1)-Cl(3)	79.60(7)
O(3)-Sm(1)-Cl(3)	138.02(5)	O(3)-Sm(1)-Cl(3)	138.27(7)
N(2)-Sm(1)-Cl(3)	110.32(6)	N(2)-Sm(1)-Cl(3)	107.69(7)
N(1)-Sm(1)-Cl(3)	74.58(6)	N(1)-Sm(1)-Cl(3)	74.63(7)
Cl(1)-Sm(1)-Cl(3)	89.52(3)	Cl(1)-Sm(1)-Cl(3)	90.91(3)
O(1)-Sm(1)-Cl(2)	75.73(5)	O(1)-Sm(1)-Cl(2)	74.95(7)
O(2)-Sm(1)-Cl(2)	153.60(6)	O(2)-Sm(1)-Cl(2)	152.65(7)
O(3)-Sm(1)-Cl(2)	135.90(5)	O(3)-Sm(1)-Cl(2)	136.15(7)
N(2)-Sm(1)-Cl(2)	74.90(5)	N(2)-Sm(1)-Cl(2)	75.08(7)
N(1)-Sm(1)-Cl(2)	116.80(5)	N(1)-Sm(1)-Cl(2)	118.74(8)
Cl(1)-Sm(1)-Cl(2)	85.73(2)	Cl(1)-Sm(1)-Cl(2)	85.00(3)
Cl(3)-Sm(1)-Cl(2)	81.76(3)	Cl(3)-Sm(1)-Cl(2)	81.40(3)

Table S2: Selected bond lengths (Å) and bond angles (deg) for $[Er(dpq)(DMF)_2Cl_3]$ (**3**) and $[Erdppz)_2Cl_3]$ (**4**)

$[Er(dpq)(DMF)_2Cl_3]$ (**3**)		$[Er(dppz)_2Cl_3]$ (**4**)	
Bond lengths (Å)		**Bond lengths (Å)**	
Er(1)-N(1)	2.558(13)	Er1-N1	2.479(3)
Er(1)-N(2)	2.519(13)	Er1-N2	2.509(3)
Er(1)-Cl(1)	2.645(4)	Er1-N5	2.503(3)
Er(1)-Cl(2)	2.599(4)	Er1- N6	2.506(3)
Er(1)-Cl(3)	2.588(4)	Er1- Cl1	2.5655(11)
Er(1)-O(1)	2.299(10)	Er1-Cl2	2.6124(12)
Er(1)-O(2)	2.303(11)	Er1-Cl3	2.6014(11)
Bond Angles (deg)		**Bond Angles (deg)**	
O(1)-Er(1)-O(2)	150.9(4)	Cl1 Er1 Cl2	88.46(4)
O(1)-Er(1)-N(2)	75.1(4)	Cl1 Er1 Cl3	89.26(4)
O(2)-Er(1)-N(2)	128.2(4)	Cl3 Er1 Cl2	160.41(3)
O(1)-Er(1)-N(1)	135.9(4)	N1 Er1 Cl1	90.95(8)
O(2)-Er(1)-N(1)	72.8(4)	N1 Er1 Cl2	77.12(8)
N(2)-Er(1)-N(1)	64.2(4)	N1 Er1 Cl3	83.47(8)
O(1)-Er(1)-Cl(3)	87.9(3)	N1 Er1 N2	65.83(10)
O(2)-Er(1)-Cl(3)	107.3(3)	N1 Er1 N5	160.19(11)
N(2)-Er(1)-Cl(3)	89.5(3)	N1 Er1 N6	130.52(11)
N(1)-Er(1)-Cl(3)	76.2(3)	N2 Er1 Cl1	153.84(8)
O(1)-Er(1)-Cl(2)	85.5(3)	N2 Er1 Cl2	97.33(8)
O(2)-Er(1)-Cl(2)	83.4(3)	N2 Er1 Cl3	76.78(8)
N(2)-Er(1)-Cl(2)	78.4(3)	N5 Er1 Cl1	84.29(8)
N(1)-Er(1)-Cl(2)	101.4(3)	N5 Er1 Cl2	121.81(8)
Cl(3)-Er(1)-Cl(2)	167.33(12)	N5 Er1 Cl3	77.26(8)
O(1)-Er(1)-Cl(1)	78.7(3)	N5 Er1 N2	113.29(11)
O(2)-Er(1)-Cl(1)	76.3(3)	N5 Er1 N6	64.55(12)
N(2)-Er(1)-Cl(1)	153.7(3)	N6 Er1 Cl1	130.12(8)
N(1)-Er(1)-Cl(1)	141.2(3)	N6 Er1 Cl2	77.84(9)
Cl(3)-Er(1)-Cl(1)	91.35(12)	N6 Er1 Cl3	117.80(9)
Cl(2)-Er(1)-Cl(1)	97.88(12)	N6 Er1 N2	76.00(10)

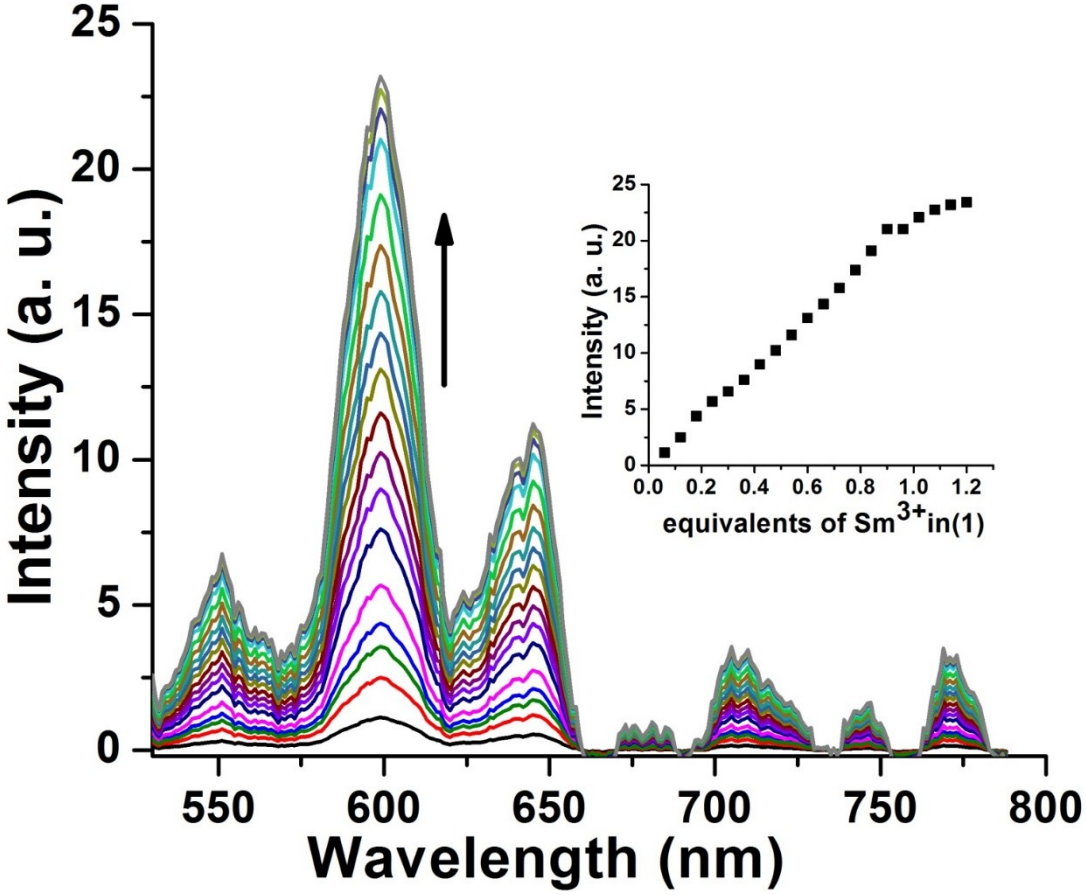

Figure 15. Time-delayed luminescence titration of $SmCl_3 \cdot 6H_2O$ in DMF upon addition of dpq in DMF solution (delay time, gate time = 0.1 ms, λ_{ex} = 340 nm, excitation slit width = 10 nm and emission slit width = 10 nm). Inset figure shows the luminescence intensity changes detected at λ_{em}= 598 nm *vs.* [Sm(III)]/[dpq]. Calculated binding constant $(K_{ML})^a = 4.86 \times 10^4\ M^{-1}$.

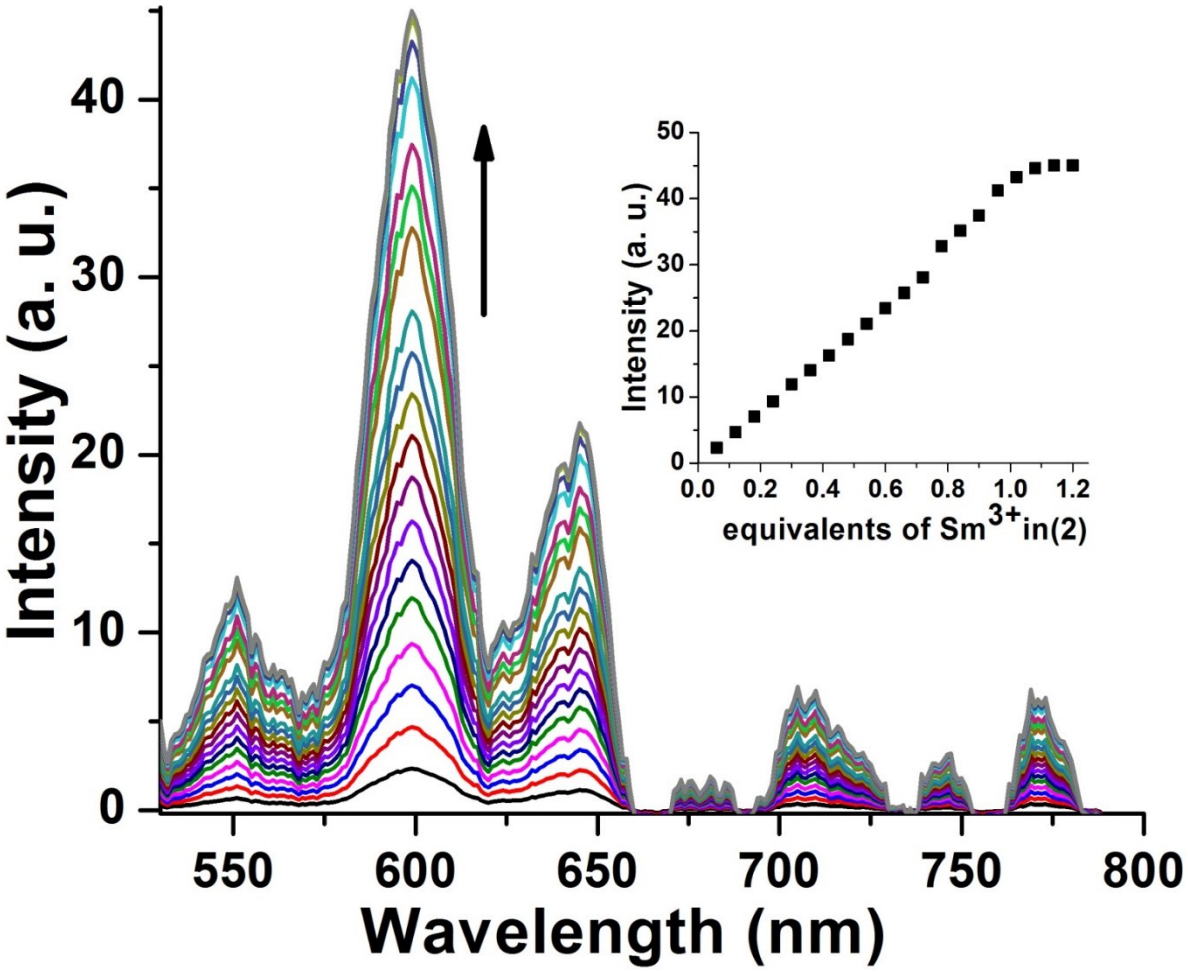

Figure 16. Time-delayed luminescence titration of $SmCl_3 \cdot 6H_2O$ in DMF upon addition of dpq in DMF solution (delay time, gate time = 0.1 ms, λ_{ex} = 340 nm, excitation slit width = 10 nm and emission slit width = 10 nm). Inset figure shows the luminescence intensity changes detected at λ_{em}= 598 nm *vs*. [$SmCl_3 \cdot 6H_2O$]/[dppz]. Calculated binding constant (K_{ML})[a] = 5.18 x 10^4 M^{-1}.

[a]Binding constants were calculated using reported procedure in (a) S. Quici, M. Cavazzini, G. Marzanni, G. Accorsi, N. Armaroli, B. Ventura, and F. Barigelletti, *Inorg. Chem,* 2005, **44**, 529-537; (b) J. Bourson, J. Pouget, and B. Valeur, *J. Phys. Chem.,* 1993, **97**, 4552-4557.

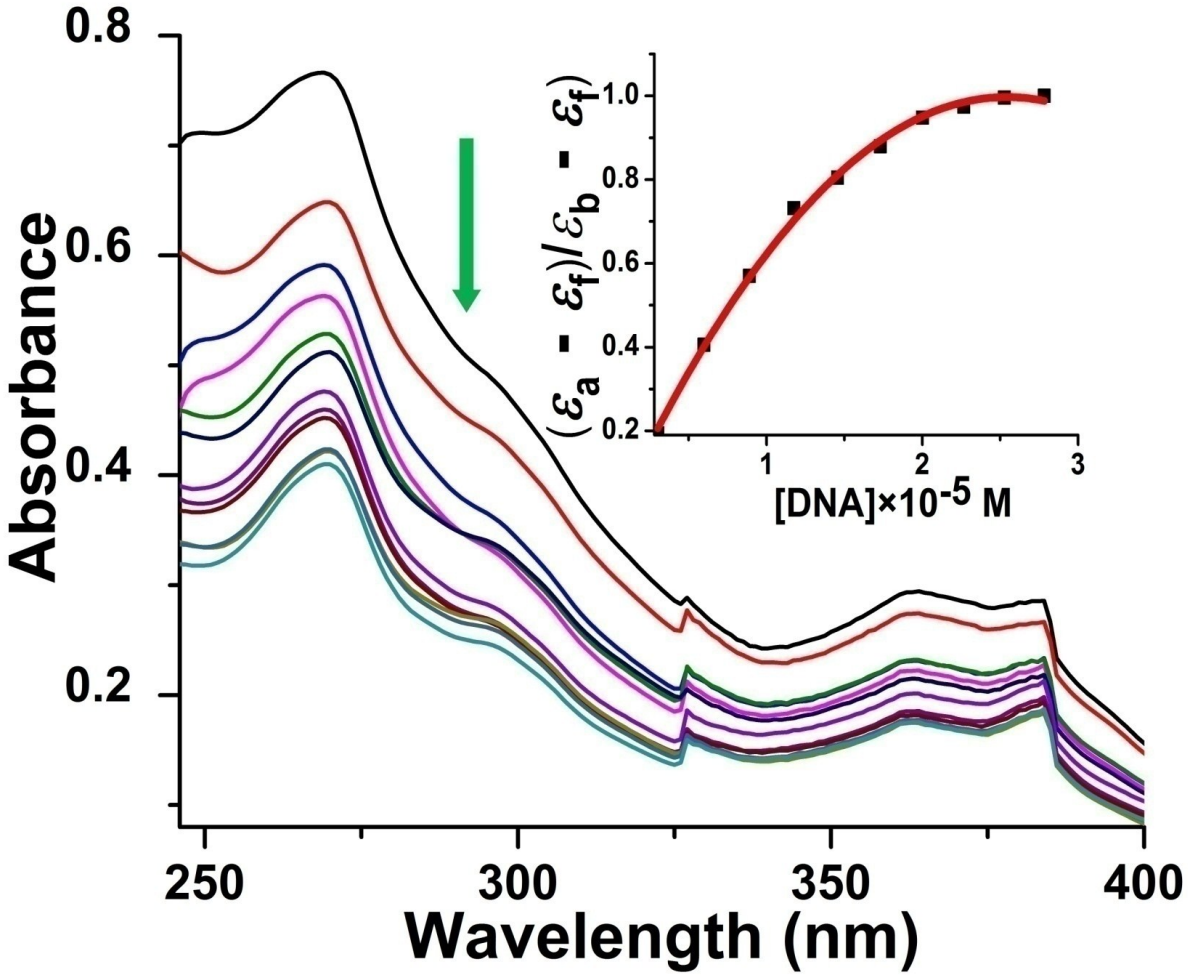

Figure 17. Absorption spectral traces of complex **2** (56 μM) in 5 mM Tris-HCl buffer (pH 7.2) with increasing the concentration of CT-DNA. Inset shows the plot of $\Delta\varepsilon_{af}/\Delta\varepsilon_{bf}$ vs. [DNA].

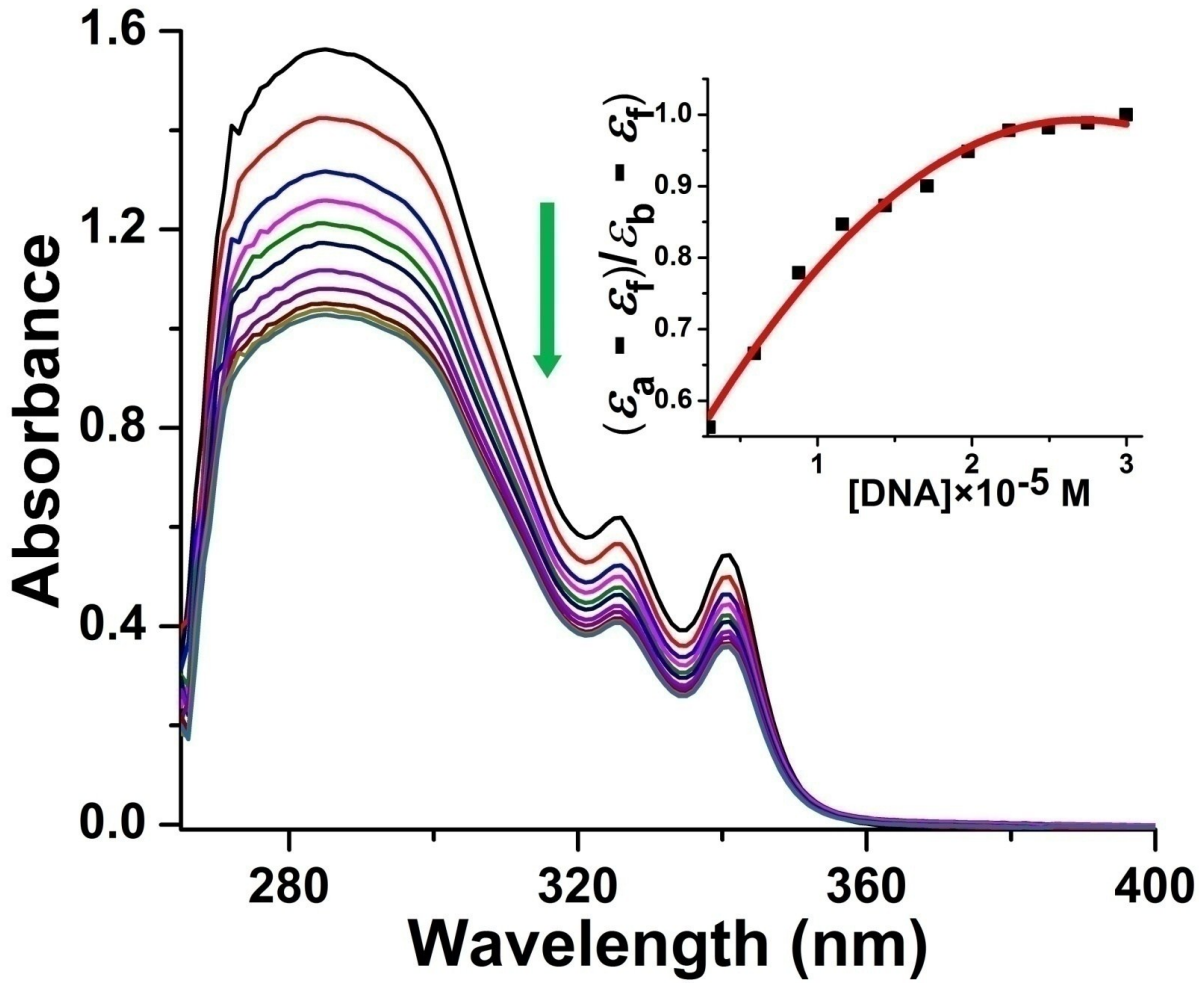

Figure S18. Absorption spectral traces of complex **3** (50 μM) in 5 mM Tris-HCl buffer (pH 7.2) with increasing the concentration of CT-DNA. Inset shows the plot of $\Delta\varepsilon_{af}/\Delta\varepsilon_{bf}$ vs. [DNA].

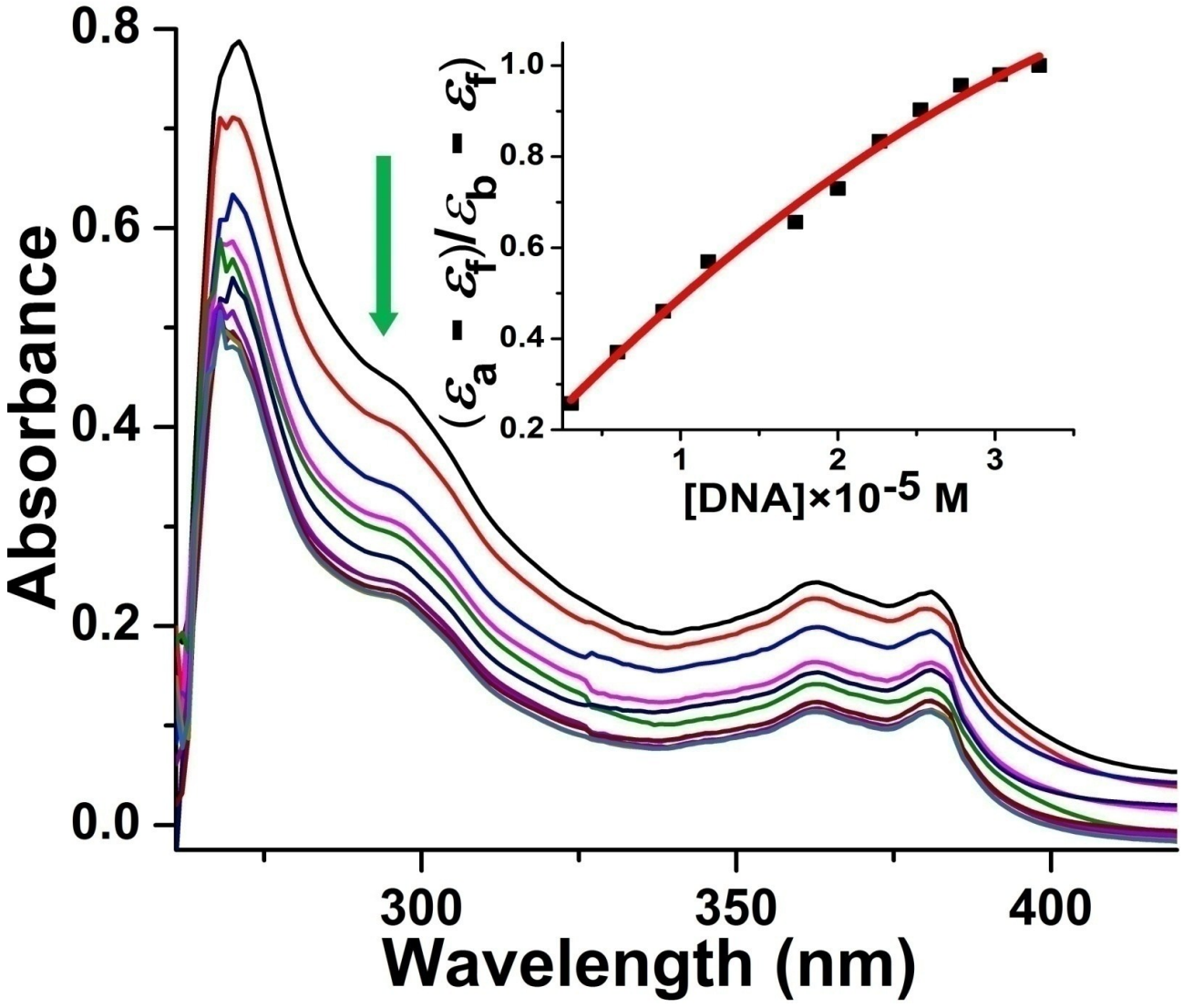

Figure S19. Absorption spectral traces of complex **4** (75 μM) in **5** mM Tris-HCl buffer (pH 7.2) with increasing the concentration of CT-DNA. Inset shows the plot of $\Delta\varepsilon_{af}/\Delta\varepsilon_{bf}$ vs. [DNA].

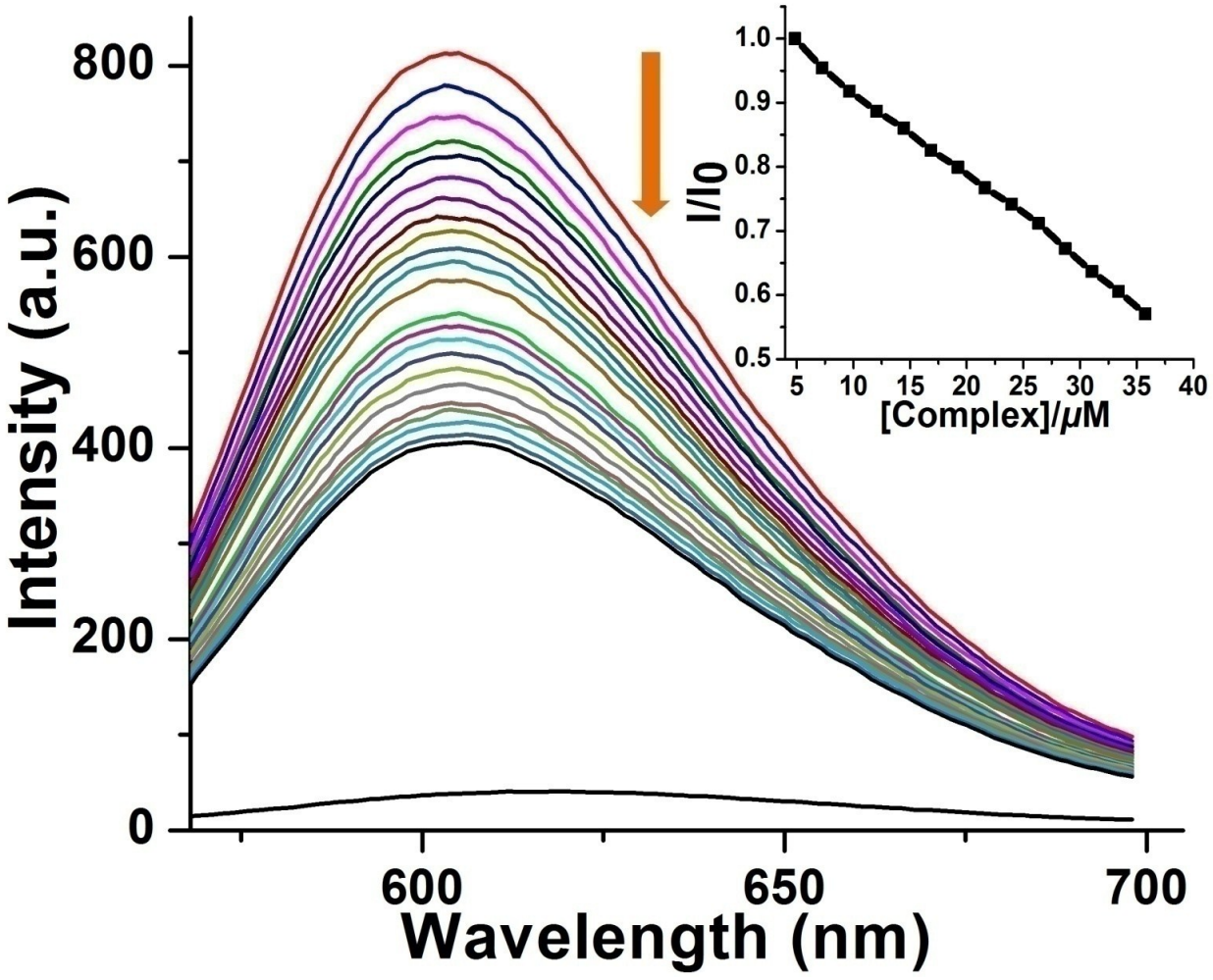

Figure S20. Emission spectral traces of ethidium bromide bound CT-DNA with varying concentration of complex **2** in 5mM Tris buffer (5 mM Tris-HCl + 5 mM NaCl, pH 7.2) at 25 °C. λ_{ex}= 546 nm, λ_{em} = 603 nm, [DNA] = 313 μM, [EthB] = 12 μM. The inset shows the plot of I/I_0 vs. [complex].

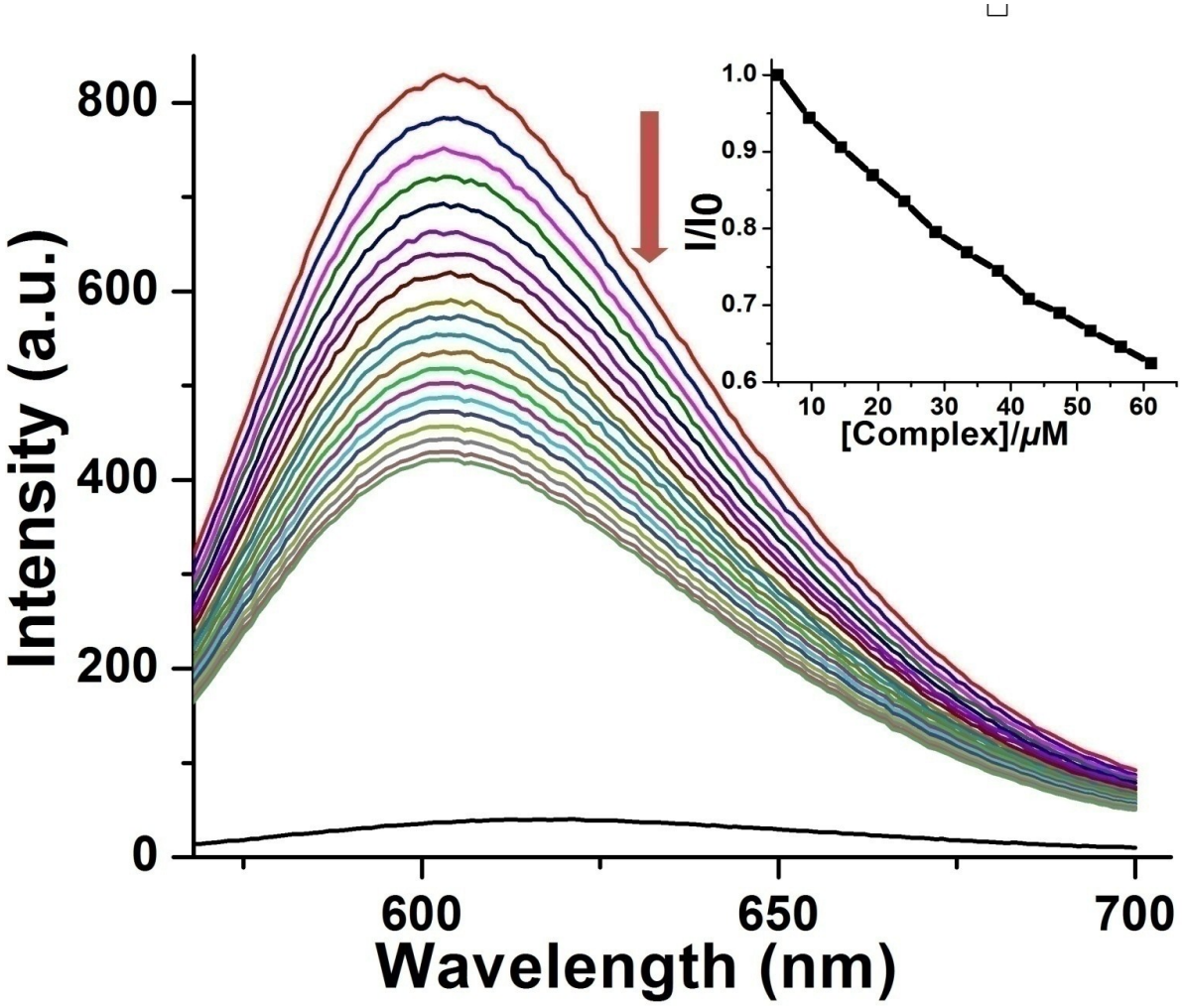

Figure S21. Emission spectral traces of ethidium bromide bound CT-DNA with varying concentration of complex **3** in 5mM Tris buffer (5 mM Tris-HCl + 5 mM NaCl, pH 7.2) at 25 °C.λ_{ex}= 546 nm, λ_{em} = 603 nm, [DNA] = 313 μM, [EthB] = 12 μM. The inset shows the plot of I/I_0 vs. [complex].

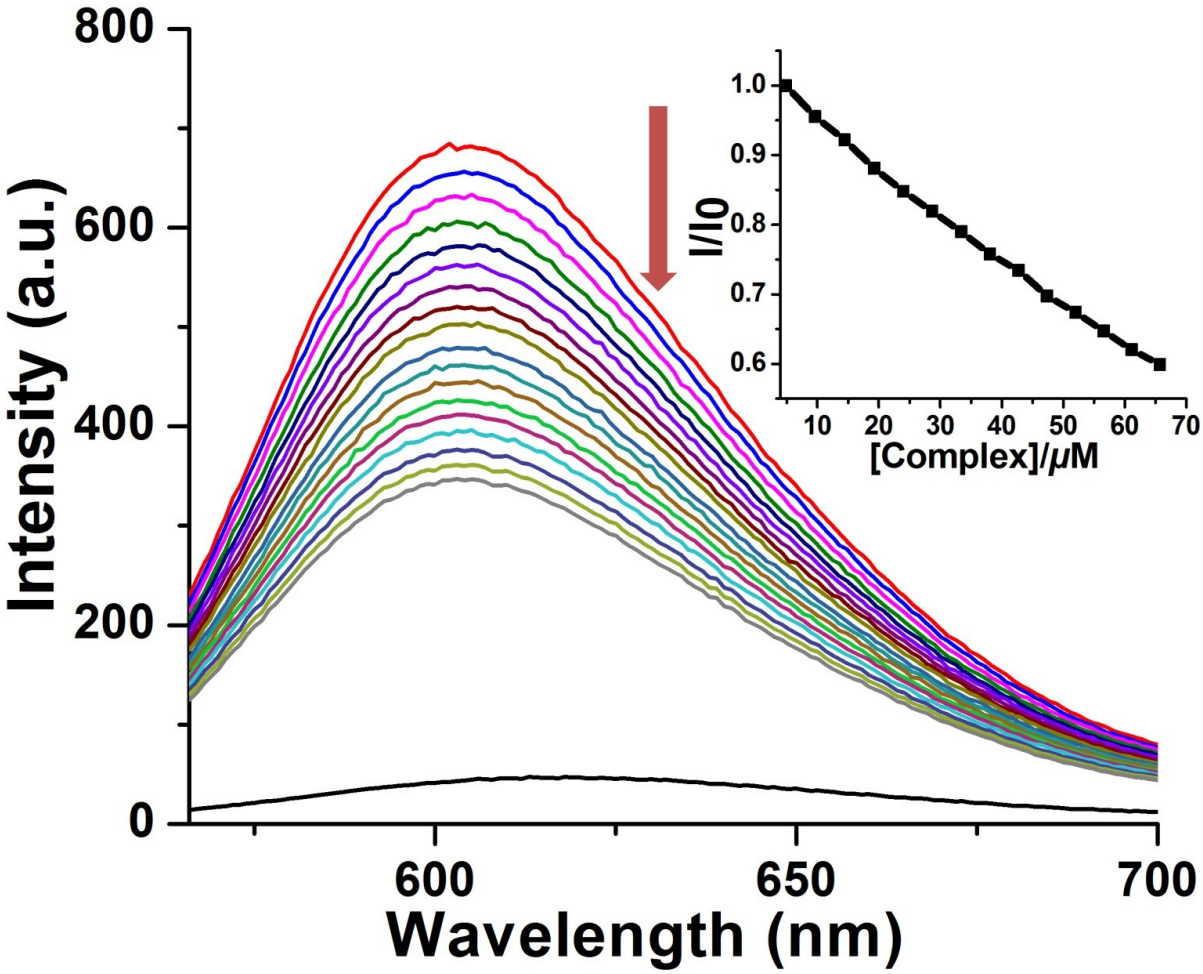

Figure S22. Emission spectral traces of ethidium bromide bound CT-DNA with varying concentration of complex **4** in 5mMTris buffer (5 mM Tris- HCl + 5 mM NaCl, pH 7.2) at 25 °C. λ_{ex}= 546 nm, λ_{em} = 603 nm, [DNA] = 313 μM, [EthB] = 12 μM. The inset shows the plot of I/I_0 vs. [complex].

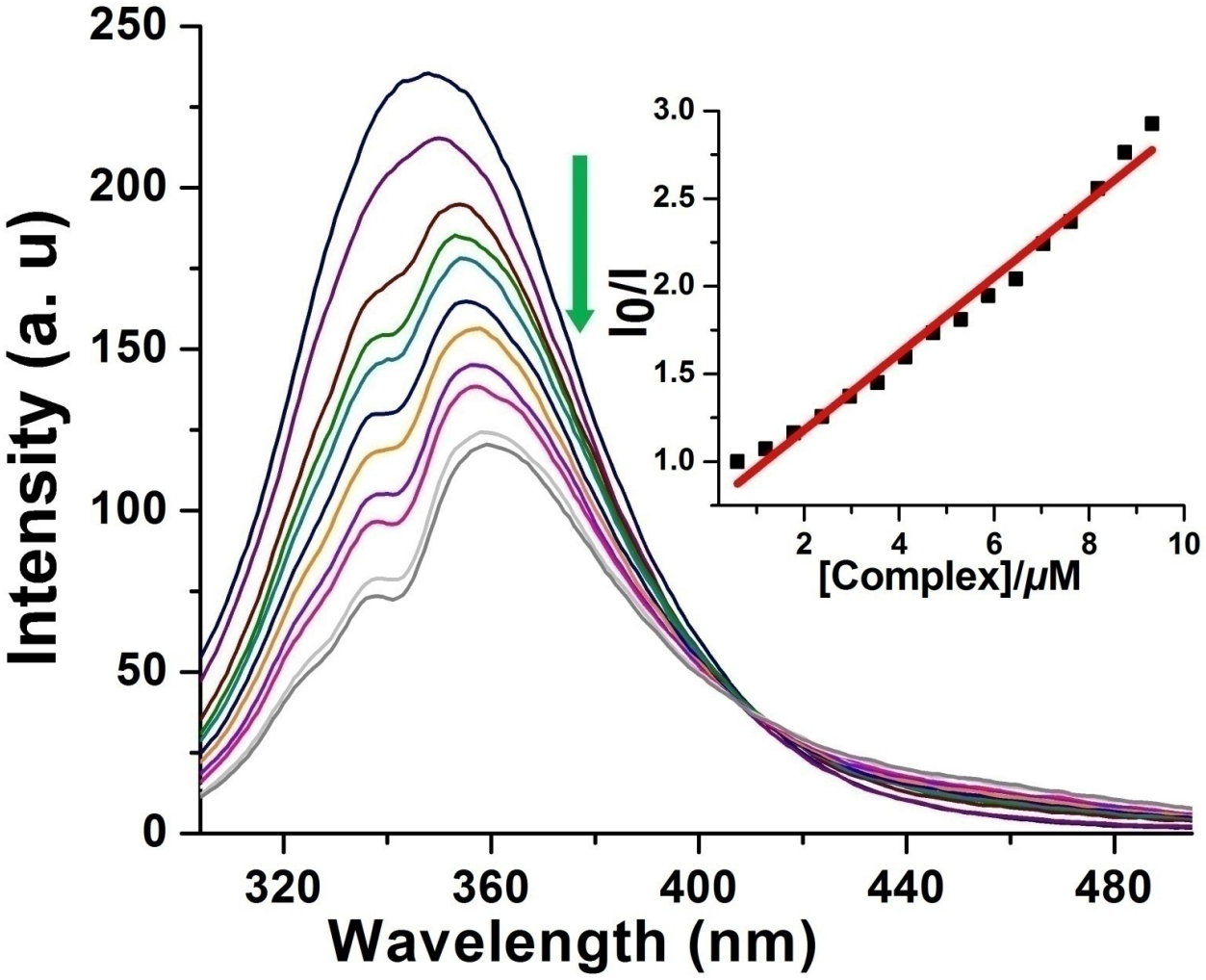

Figure S23. Emission spectral traces of bovine serum albumin (BSA) protein (5 μM) in the presence of complex **1**. The arrow shows the intensity changes on increasing complex concentration. The inset shows the plot of (I_0/I) *vs*. [complex].

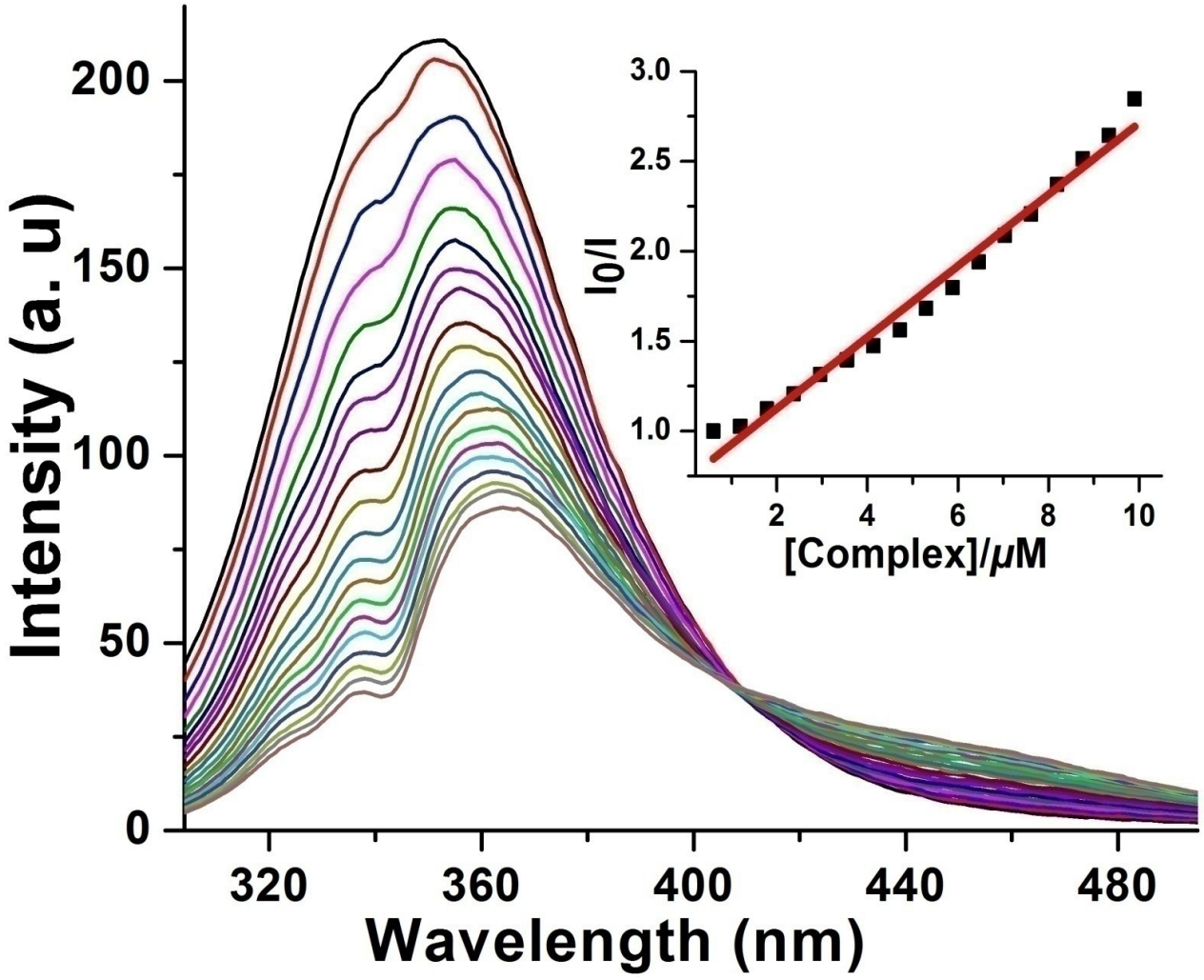

Figure S24. Emission spectral traces of bovine serum albumin (BSA) protein (5 μM) in the presence of complex **3**. The arrow shows the intensity changes on increasing complex concentration. The inset shows the plot of (I_0/I) vs. [complex].

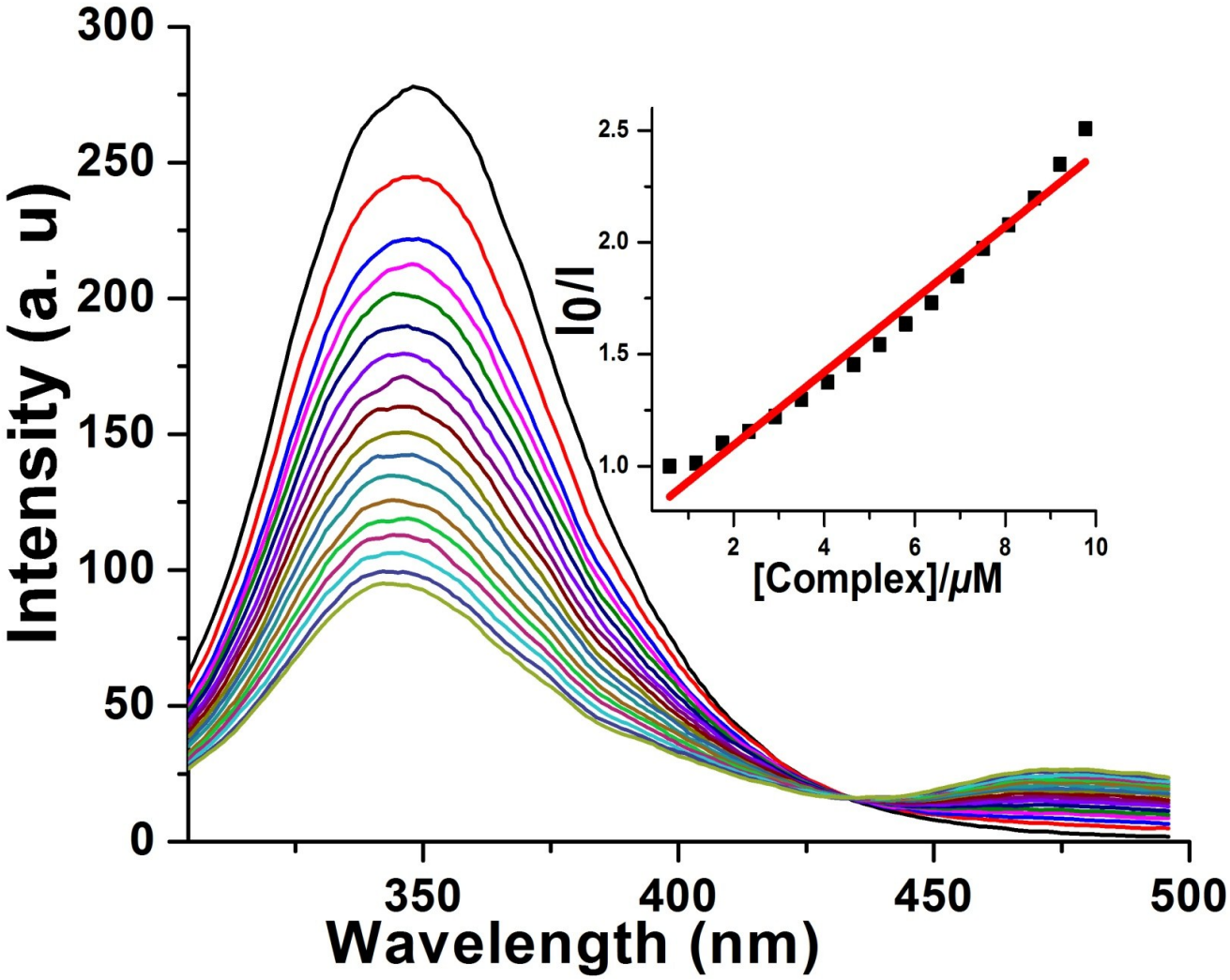

Figure S25. Emission spectral traces of bovine serum albumin (BSA) protein (5 μM) in the presence of complex **4**. The arrow shows the intensity changes on increasing complex concentration. The inset shows the plot of (I_0/I) vs. [complex].

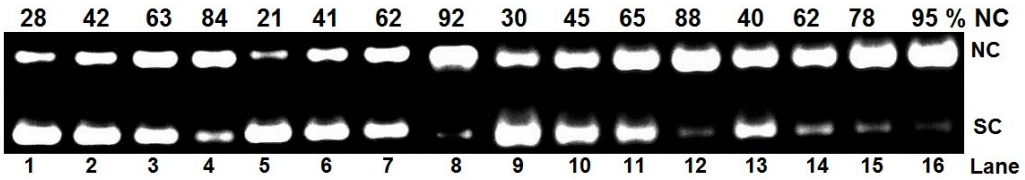

Figure S26. Gel electrophoresis diagram showing the cleavage of SC pUC19 DNA (30μM, 0.2μg) incubated with complexes **1-4** (20 μM) in 50 mM Tris-HCl/NaCl buffer (pH, 7.2) at 37 ^{0}C for 1 h on irradiation with UV-A light of 365 nm (6 W) at different time. Detailed conditions are given below in a tabular form.

Lane No.	Reaction Condition	λ/nm	Exposure time (t/min)	%NC
1	DNA+**1**	365	30	28
2	DNA+**1**	365	60	42
3	DNA+**1**	365	90	63
4	DNA+**1**	365	120	84
5	DNA+**2**	365	30	21
6	DNA+**2**	365	60	41
7	DNA+**2**	365	90	62
8	DNA+**2**	365	120	92
9	DNA+**3**	365	30	30
10	DNA+**3**	365	60	45
11	DNA+**3**	365	90	65
12	DNA+**3**	365	120	88
13	DNA+**4**	365	30	40
14	DNA+**4**	365	60	62
15	DNA+**4**	365	90	78
16	DNA+**4**	365	120	95

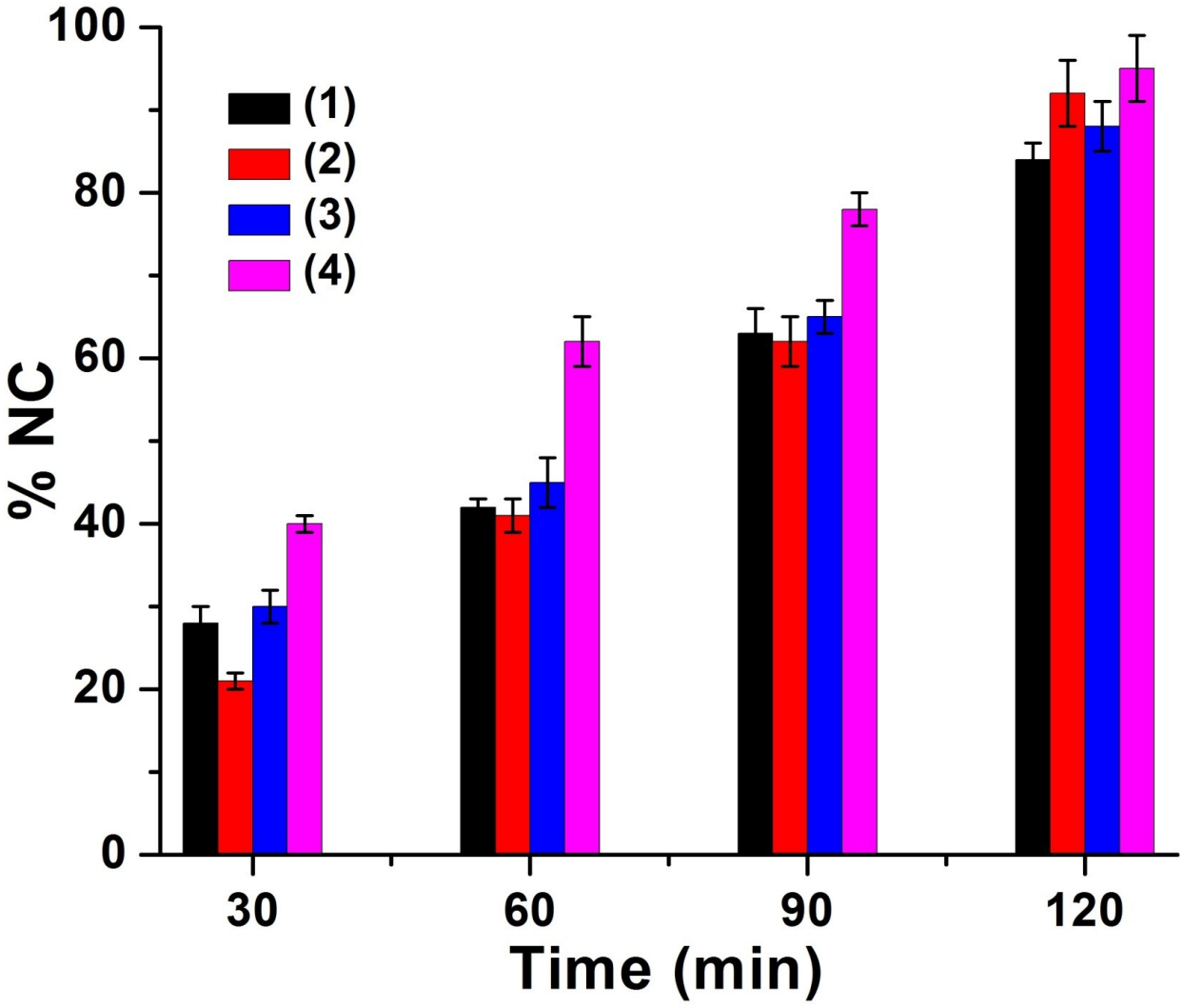

Figure S27. Bar diagram showing the photocleavage of SC pUC19 DNA (30μM, 0.2μg) with complexes **1-4** (20 μM) in 50 mM Tris-HCl/NaCl buffer (pH, 7.2) on irradiation with UV-A light of 365 nm (6 W) with varying time. The plot was made with data from gel electrophoresis diagram in Fig. S28.

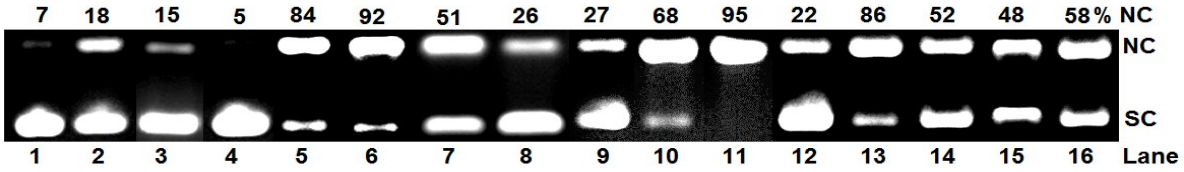

Figure S28. Gel electrophoresis diagram showing the cleavage of SC pUC19 DNA (30μM, 0.2μg) incubated with complexes **1** and **2**(20 μM) in 50 mM Tris-HCl/NaCl buffer (pH, 7.2) at 37 ^{0}C for 1 h on irradiation with UV-A light of 365 nm (6 W) for 2 h: lane 1, DNA control; lane 2, DNA + dpq (20 μM); lane 3, DNA + dppz (20 μM); lane 4, DNA + $SmCl_3 \cdot 6H_2O$ (20 μM); lane 5, DNA + **1**; lane 6, DNA + **2**; lane 7, DNA + **1** + DMSO (4 μL); lane 8, DNA + **1**+ KI (200 μM); lane 9, DNA + **1** + NaN_3 (400 μM); lane 10, DNA + **1** + L-histidine (400 μM); lane 11, DNA + **1** + D_2O (16 μL); lane 12, DNA + methyl green (200 μM); lane 13, DNA + **1**+ methyl green (200 μM); lane 14,DNA + **1** + catalase (200 μM); lane 15, DNA + **2** + methyl green (200 μM); lane 16, DNA + **2** + catalase (200 μM).

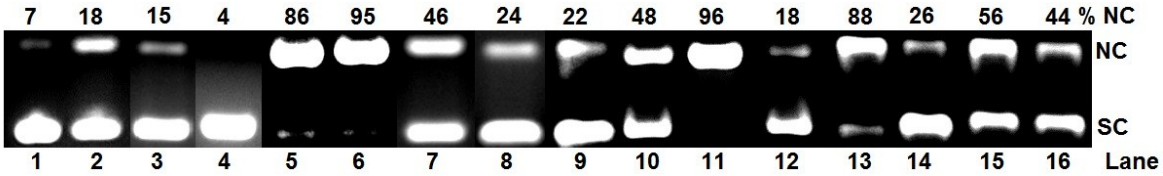

Figure S29. Gel electrophoresis diagram showing the cleavage of SC pUC19 DNA (30μM, 0.2μg) incubated with complexes **3** and **4** (10 μM) in 50 mM Tris-HCl/NaCl buffer (pH, 7.2) at 37 ^{0}C for 1 h on irradiation with UV-A light of 365 nm (6 W) for 2 h: lane 1, DNA control; lane 2, DNA + dpq (20 μM); lane 3, DNA + dppz (20 μM); lane 4, DNA + $SmCl_3 \cdot 6H_2O$ (20 μM); lane 5, DNA + **3**; lane 6, DNA + **4**; lane 7, DNA + **4** + DMSO (4 μL); lane 8, DNA + **4** + KI (200 μM); lane 9, DNA + **4** + NaN_3 (400 μM); lane 10, DNA + **4** + L-histidine (400 μM); lane 11, DNA + **4** + D_2O (16 μL); lane 12, DNA + methyl green (200 μM); lane 13, DNA + **3** + methyl green (200 μM); lane 14, DNA + **4** + methyl green (200 μM); lane 15, DNA + **3** + catalase (200 μM); lane 16, DNA + **4** + catalase (200 μM).

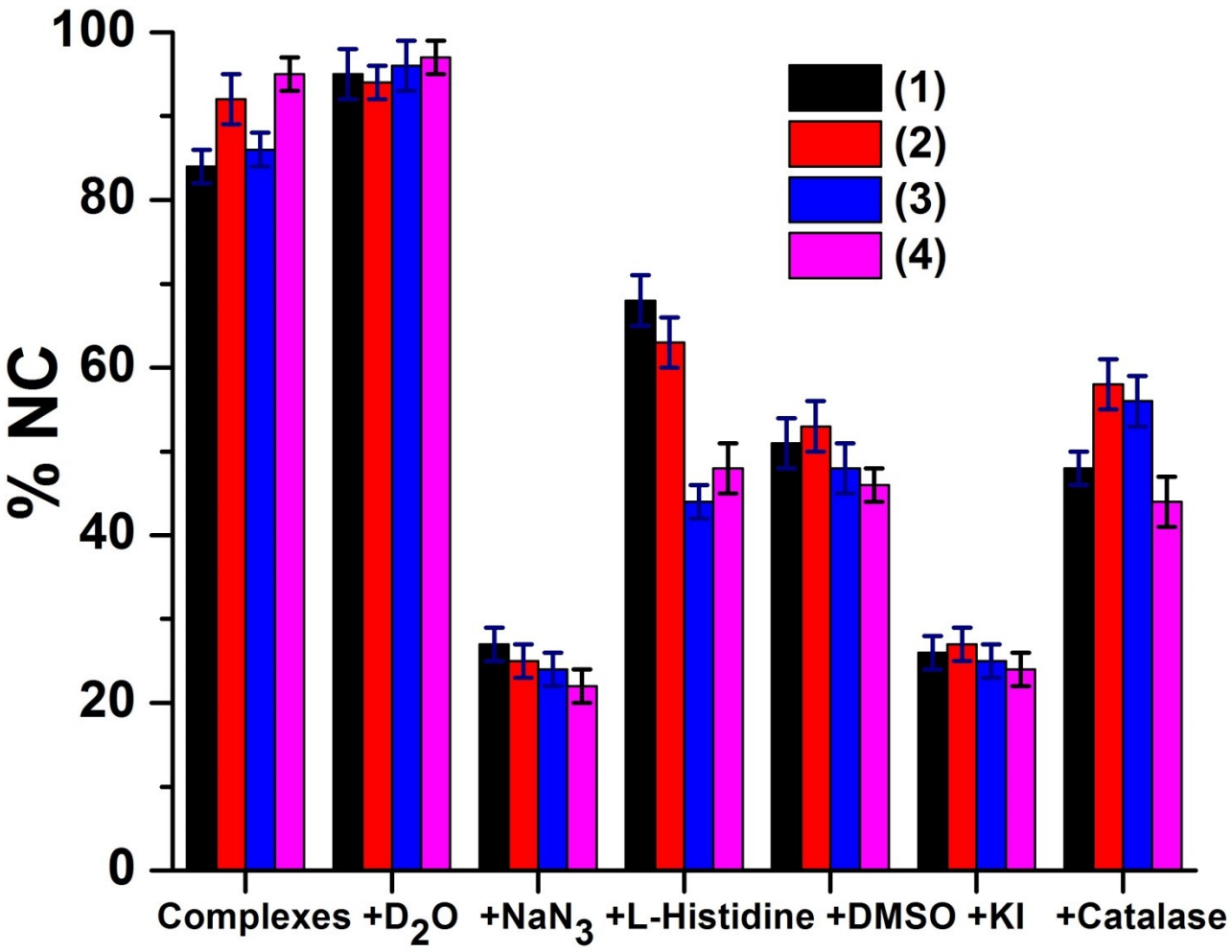

Figure S30. Bar diagram of for the cleavage of SC pUC19 DNA (30 μM, 0.2 μg) by complexes **1**-**4** (20 μM) on photoexposure at 365 nm(6W) for 2 h in the presence of various additives in Tris-HCl/NaCl buffer. The additive concentrations/quantities are NaN_3, 0.2mM; KI, 0.2 mM; D2O, 16 μL; L-histidine, 0.2 mM; DMSO, 4μL; Catalase, 4 units.